

7. SEDIMENTARY STRUCTURES OF CONTOURITES AND TURBIDITES OBSERVED BY X-RADIOGRAPHIC PRINTS: SAMPLES FROM BLAKE-BAHAMA OUTER RIDGE AND SOHM ABYSSAL PLAIN¹

M. Yokokawa²

ABSTRACT

X-radiographic prints were made from slab samples to investigate sedimentary structures collected from drift deposits drilled along the Blake-Bahama Outer Ridge and Sohm Abyssal Plain during Ocean Drilling Program Leg 172.

All samples are composed of fine-grained silt- and clay-sized sediments, except the foraminiferal sand. The sediments are mixtures of components such as carbonate (nannofossils and foraminifers) and siliclastic sediments. Samples can be divided into two groups: (1) samples containing distinct sedimentary structures derived from such episodic currents as turbidity currents or benthic storms (Group I) and (2) samples containing sedimentary structures associated with changes in color or magnetic susceptibility but not associated with the distinct structures in visual inspections compared to Group I (Group II). Group II is considered to represent more common sedimentary processes in this region because the frequency of occurrence of these structures is much higher than that of Group I.

X-radiographic prints revealed more detailed sedimentary structures compared to visual inspections for Group I sediments. For Group II sediments, it was revealed that changes in color or magnetic susceptibility are sometimes associated with line structures even though they are not observed in visual inspections. Detailed descriptions of these sedimen-

¹Yokokawa, M., 2001. Sedimentary structures of contourites and turbidites observed by X-radiographic prints: samples from Blake-Bahama Outer Ridge and Sohm Abyssal Plain. *In* Keigwin, L.D., Rio, D., Acton, G.D., and Arnold, E. (Eds.), *Proc. ODP, Sci. Results*, 172, 1–37 [Online]. Available from World Wide Web: <http://www-odp.tamu.edu/publications/172_SR/VOLUME/CHAPTERS/SR172_07.PDF>. [Cited YYYY-MM-DD]

²Department of Earth and Space Science, Osaka University, Toyonaka, Osaka 560-0043, Japan.
miwa@user.center.osaka-u.ac.jp

tary structures are given in this paper. Although further investigation is needed to discover the intensity of the currents that formed these structures, the features observed here aid our understanding of sedimentation in the deep-sea environment.

INTRODUCTION

During Ocean Drilling Program (ODP) Leg 172, drift deposit sediments were drilled along the Blake-Bahama Outer Ridge and Bermuda Rise. Drilling at Sohm Abyssal Plain was attempted but was interrupted. Contour currents, such as the Deep Western Boundary Current associated with the production of the North Atlantic Deep Water and Antarctic Bottom Water, supply sediments to the Blake-Bahama Outer Ridge and Bermuda Rise, resulting in high sedimentation rates. The maximum average sedimentation rate reached 47.12 cm/k.y. at Site 1061 during marine isotope Stages 2–4 (see Keigwin, Rio, Acton, et al., 1998, chap. 5, fig. 64). We are interested in discovering what kind of sedimentary processes can result in such amazingly high sedimentation rates in deep-sea environments. Although there have been studies of geochemistry and grain-size variations (e.g., Keigwin and Jones, 1989; Johnson et al., 1988; Haskell et al., 1991), sedimentary structures themselves have been paid less attention in this region.

Distinct sedimentary structures have been observed at Leg 172 sites. Research by the high-energy benthic boundary layer experiment (HEBBLE) (e.g., Nowell and Hollister, 1985) showed that fairly intense storms occur in the deep-sea environment. In light of these benthic storms, the sedimentary structures observed at our sites could become a key to understanding the sedimentary processes associated with contour currents in the deep-sea environment. This paper will introduce and give detailed descriptions of some examples of sedimentary structures observed at these sites.

METHODS

Sampling

For the purpose of observing sedimentary structures in detail, slab samples were taken to make X-radiographic prints (Table T1). Some of the slab samples were collected on board ship for visibly distinct sedimentary structures. The other slab samples were collected at the Bremen Core Repository after the cruise. These samples were chosen to investigate the sedimentary structures associated with significant changes in sediment color or magnetic susceptibility in marine isotope Stages 8–10. The slab samples are either 15 cm × 3 cm × 1 cm or 10 cm × 3 cm × 1 cm. The slab samples were taken using thin metal frames. The samples were carefully wrapped in thin transparent plastic to avoid drying and breaking.

X-Radiography

X-radiographic prints were made by a “soft” (i.e., relatively long wavelength) X-ray generator, Sofron Type STA-1005 (SOFRON Co. Ltd.), at the Geological Survey of Japan. The plastic-wrapped slab samples were placed directly on an exposure holder that contains photographic

T1. List of slab samples and conditions of X-radiographic prints, p. 37.

printing paper and an intensifying screen (Kyokko SMP-308, Kasei Optonix, Ltd.). Black-and-white photographic printing papers (Fujibro WP FM3, 25.4 cm × 30.5 cm, medium weight, white, glossy, hard paper, Fuji Photo Film Co. Ltd.) were used. The exposure holder, above which a sample was placed, was mounted ~0.6 m below the X-ray source. The X-ray current was 4 mA. Other conditions, such as voltage and exposure time, were controlled for each sample so that the internal sedimentary structures could be observed clearly. These conditions are shown in Table T1. After the X-ray exposure was finished, the photographic printing paper was taken out of the exposure holder and processed in a darkroom like a regular photograph.

Because the X-radiographic prints were made directly onto the photographic printing paper in this procedure, the prints are negative, which means the darker regions represent the more penetrable parts of the sample and the lighter regions the more opaque areas (e.g., Bouma, 1969). High atomic number elements absorb the radiation much more strongly than low atomic number elements, and more dense elements absorb more radiation than those that are less dense (e.g., Young, 1967).

Description

“Results,” p. 3, contains descriptions of the samples and their X-radiographic prints. The sample descriptions, regarding such elements as sediment color (compared with Munsell soil color charts) (Munsell, 1975) and grain size, are based on the visual core descriptions given in the Leg 172 *Initial Reports* volume (Keigwin, Rio, Acton, et al., 1998). Magnetic susceptibility and color reflectance values are described based on shipboard measurements (Keigwin, Rio, Acton, et al., 1998) when there are significant changes in those values.

Color reflectance was measured using a Minolta spectrophotometer (Minolta CM-2002), and results are expressed in the L*a*b* color system. The L*a*b* system can be visualized as a cylindrical coordinate system in which the axis of the cylinder is the lightness variable L*, ranging from 0% to 100%, and the radii are the chromaticity variables a* and b*. Variable a* is the green (negative) to red (positive) axis, and variable b* is the blue (negative) to yellow (positive) axis (Blum, 1997).

RESULTS

Samples can be divided into two groups (Table T1). Group I contains distinct sedimentary structures derived from such episodic currents as turbidity currents or benthic storms, and Group II contains sedimentary structures associated with a change in color or magnetic susceptibility but not associated with distinct structures in visible inspections compared to Group I. Group II is considered to represent more common sedimentary processes in this region because the frequency of occurrence of these structures is much higher than that of Group I.

In general, features observed on the radiographs are (1) the images getting lighter as the nannofossil (CaCO₃) content increases and (2) the images getting lighter as the sediments become coarser. In the following sections, characteristic features observed in X-radiographic prints are described in detail. In this paper, the sediments are described starting at the base of a section and proceeding uphole.

Group I

Site 1055

Sample 172-1055D-6H-1, 84–99 cm (44.44–44.59 mbsf: 51.06–51.21 mcd; Marine Isotope Stage 8)

This sample was taken where interbedded silt layers and dark greenish gray (8.5Y 4.8/1.5) clayey silt scour the underlying light greenish gray (2.7GY 5.1/1.3) silty clay (Fig. F1). Magnetic susceptibility values show a relatively large fluctuation in this interval (Fig. F2). Color reflectance values, especially L* and b*, also show a large change in this interval (Fig. F3).

Description of X-Radiographic Print. The characteristic features of this sample are sharp surfaces, which can be interpreted as erosional surfaces, and distinct sharp lines associated with upward gradation of shading in the radiograph, which seems to show fining-upward structures (Fig. F4).

According to the visual core description, the lowermost 0.9-cm-thick layer (Fig. F4, interval a) is massive silty clay. This silty clay is eroded by upper layers. The 2.2-cm interval above this erosional surface (Fig. F4, interval b) contains distinct, sharp light-colored lines. These distinct lines show that the silty sediments were deposited as plane beds. The lower 1.2 cm of this interval (Fig. F4, interval b₁), in particular, consists of four layers with lower boundaries that are sharp and bright but gradually darken a few millimeters uphole. This feature in the radiograph seems to show fining-upward structures, although these fining-upward structures were not recognized in visual inspection of the core (Fig. F1). The 1.6-cm interval above this zone (Fig. F4, interval c) is structureless. Further uphole, the 2.2-cm interval consists again of distinct lines showing fining-upward structures (Fig. F4, interval d). The top of this zone is an erosional surface (the boundary between intervals d and e in Fig. F4).

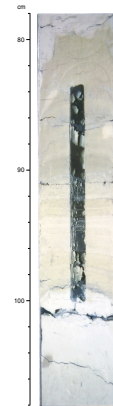
The interval from 90.2 to 92.0 cm (Fig. F4, interval e) consists of coarser sediments. Sharp lines observed in the radiograph seem to show that the coarser material was deposited as discrete beds. The upper contact of this zone is also an erosional surface, but it is fairly undulated. In a 3.0-cm interval above this erosional surface are fining-upward layers ~3 mm in thickness (Fig. F4, interval f). The upper contact of this zone is also a sharp erosional surface that is overlain by coarser material ~1.5 cm thick (Fig. F4, interval g). These coarser sediments do not show distinct sedimentary structures relative to interval e. Further uphole, the uppermost 1.5 cm of this sample shows distinct lines that are destroyed at the center of the core by bioturbation (Fig. F4, interval h). Except for this interval, no significant bioturbation is recognized elsewhere in this sample, which suggests that this 15-cm interval was deposited in a short time.

Site 1056

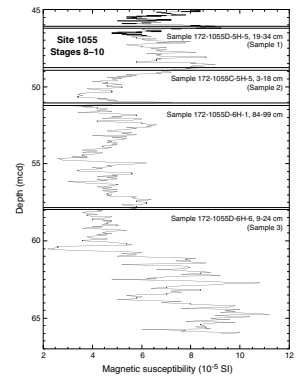
Intervals 172-1056B-6H-5, 51–66 cm, and 69–79 cm (48.14–48.42 mbsf: 54.09–54.37 mcd; Marine Isotope Stages 13–15)

Distinct sedimentary structures consisting of coarser sediments are not often found in the upper part of Unit I at Site 1056 but are present below 48 mbsf. Sample 172-1056B-6H-5, 51–79 cm (Fig. F5) is a most distinct one (Keigwin, Rio, Acton, et al., 1998, chap. 4, fig. 2). In the lowermost part of the sample (i.e., at 78.5 cm), greenish gray (5GY 5/1)

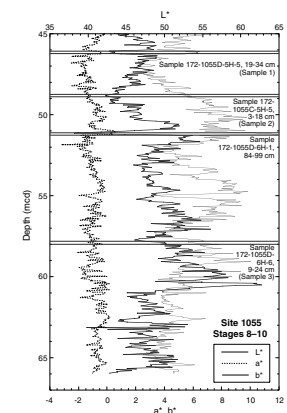
F1. Close-up photograph containing interbedded silt layers and dark greenish gray clayey silt, p. 14.



F2. Magnetic susceptibility variation with depth at Site 1055 during marine isotope Stages 8–10, p. 15.



F3. Color reflectance variation with depth at Site 1055 during marine isotope Stages 8–10, p. 16.

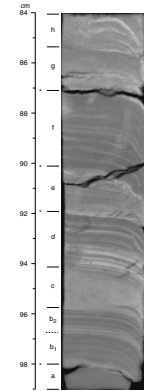


nannofossil clay is scoured sharply by coarser beds of grayish olive (10Y 4/2) sand-sized siliciclastic and biogenic components interbedded with silt and clay. Magnetic susceptibility values show sharp peaks (Fig. F6).

Description of X-Radiographic Print. The lowermost erosional surface is a sharp boundary (Fig. F7B, between intervals a and b), although there is a crack at that contact. Directly above this erosional surface (Fig. F7B, interval b), there are three fining-upward layers between 77.4 and 78.5 mbsf (Fig. F7B, interval b₁) in the X-radiographic print, although only two layers can be recognized by visual inspection of the split core (Keigwin, Rio, Acton, et al., 1998, chap. 4, fig. 2). The lowermost layer contains a series of very thin lines, suggesting the existence of multiple plane beds. Around 76 cm in this section (Fig. F7B, interval c), visual core inspection reveals a pair of distinct fining-upward layers; however the X-radiographic print shows that the lower layer (Fig. F7B, interval c₁) consists of three fining-upward layers, and furthermore, the lowest layer in interval c₁ contains a dipping structure like ripple cross-laminae. Above these layers, there is a 1.3-cm-thick clay layer (Fig. F7B, interval d) containing sharp “hairlines”, which are very thin but clear light-colored lines. Further upcore, three fining-upward layers are recognized (Fig. F7B, interval e) and the X-radiographic print shows that the middle layer contains ripple cross-laminae that are 2 mm high (at 73.8 cm). The overlying clay layer (Fig. F7B, interval f) consists of two fining-upward layers and is truncated by overlying coarser layers (Fig. F7B, interval g) that contain dipping cross-laminae. These coarser layers are overlain by a 2-mm-thick mud layer (Fig. F7B, interval h). This clay layer is again overlain by coarser sediments (Fig. F7B, interval i), which thin laterally. The uppermost clayey part (Fig. F7B, interval j) of the interval contains sharp, distinct lines every 2–3 mm that are not clear in visual inspection of the core. Little bioturbation occurs in the interval from 69–79 cm, suggesting that multiple deposition events occurred over a relatively short time.

There is a gap of 3 cm between the intervals shown in Figures F7A and F7B that contains a clay layer continued from the fining-upward layer at the upper end of the lower interval (Fig. F7B, above interval j; shown only in the right part). Thin silt layers appear in the upper part of this clay layer, which are observed in the lowermost part of the interval shown in Figure F7A, interval l, as two light lines. Some burrows filled with silt- and sand-sized materials are observed directly above these silt layers in the close-up photograph (Keigwin, Rio, Acton, et al., 1998, chap. 4, fig. 2). This clay layer in the lowermost part of Figure F7A, interval l, is overlain by 7.6 cm of silt- and sand-sized sediments (Fig. F7A, interval m; 56.9–64.5 cm) including mud clasts. In the X-radiographic print, the lowermost 0.7 cm of this interval (Fig. F7A, interval m₁) is slightly lighter-colored and seems to be a little bit coarser material. The overlying 1.9-cm interval (Fig. F7A, interval m₂) seems to have plane beds, although they are not clearly defined. There is a burrow in the lower part of this interval. The upper 5-cm interval (Fig. F7A, intervals m₃, m₄) contains clear lines, suggesting plane bed formation during deposition, but the uppermost 2 cm (Fig. F7A, interval m₄) seems to be slightly bioturbated. This coarser interval (Fig. F7A, intervals m₁–m₄) is overlain by a clayey layer (nannofossil clay mixed sediments) interbedded with silt layers (Fig. F7A, interval n). Linear structures appear in the X-radiographic print in this interval. The uppermost 2.5 cm (Fig. F7A, interval o) of figure F7A consists of a bioturbated clay-sized sediment (nannofossil clay mixed sediments) layer that

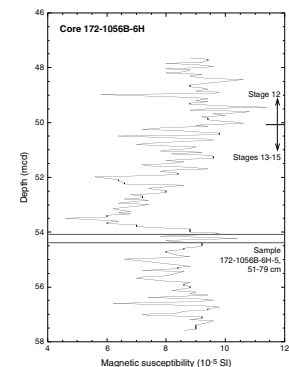
F4. X-radiographic print showing major erosional surfaces, p. 17.



F5. Close-up photograph containing a sequence of coarser beds of sand-sized siliciclastic and biogenic components interbedded with silt and clay, p. 18.



F6. Magnetic susceptibility variation with depth, p. 19.



becomes gradually lighter in the radiograph. The lower, coarser part of the sample (Fig. F7A, interval m) seems to have been deposited quickly, and this fast deposition of coarse material seems to end gradually toward the uppermost part of this sample.

Site 1059

Sample 172-1059C-7H-6, 41–56 cm (64.91–65.06 mbsf; 75.17–75.32 mcd; Marine Isotope Stage 8)

This interval includes the silt layer that is situated in early marine isotope Stage 8 and is correlatable from Sites 1055 to 1062. Silt layers, <1 mm thick, are observable by visual inspection (Keigwin, Rio, Acton, et al., 1998, chap. 4, fig. 13). The silt layers are interbedded in the interval of light greenish gray (2.5GY 5/1) nannofossil clay and are overlain by greenish gray (7.2Y 4/1) clay with silt and nannofossils. Magnetic susceptibility shows a peak in this interval (Fig. F8), and L* color reflectance values show a negative peak (Fig. F9).

Description of X-Radiographic Print. The silt layers are observed as bright lines ~2–3 cm above the bottom of the sample (Fig. F10, interval b). These lines show lateral changes in lightness, possibly because of the coarseness of the silt grains. These silt layers are overlain by a slightly bioturbated 1.3-cm-thick clay layer (Fig. F10, interval c). The silt layers, which overlie the clay layer, consist of three layers (Fig. F10, interval d). The top layer appears clearest compared to the lower two layers. These silt layers are overlain by a bioturbated 1-cm-thick clay layer (Fig. F10, interval e). This clay layer is again scoured sharply by the silt layer at 49.7 cm in depth. This silt layer appears most clearly in the radiograph. Above this silt layer, at least five sharp hairlines are observed in the X-radiographic print, although they are bioturbated a little (Fig. F10, interval f). The remaining upper part of this sample (Fig. F10, interval g) is heavily bioturbated so that no clear structures are observed. This set of silt layers (49–55 cm) may have been deposited by multiple events that occurred over a relatively short time.

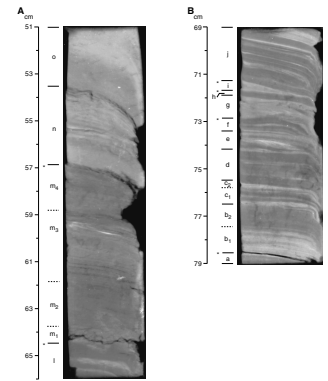
Site 1062

Sample 172-1062A-15H-3, 115–125 cm (129.85–129.95 mbsf; 138.31–138.41 mcd; ~1.4 Ma)

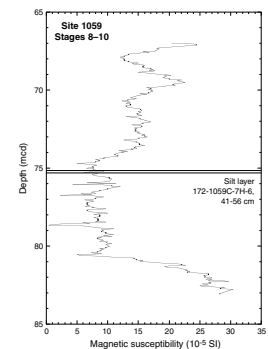
Unit II in Hole 1062A (75–150 mbsf) often includes carbonate turbidites, which consist of well-preserved foraminifers (e.g., Keigwin, Rio, Acton, et al., 1998, chap. 5, fig. 10). The overlying Unit I does not include foraminiferal sand. The foraminiferal sand layers (i.e., carbonate turbidites) appear again at 177 mbsf and in the deeper part of Unit III in Hole 1062B as well. These carbonate turbidites appear at both the eastern and western flanks, and some of them can be correlated to each other (Keigwin, Rio, Acton, et al., 1998, chap. 5, table 3). These carbonate turbidites become thinner downhole, and this sample is taken from one such thin layer (Fig. F11). By visual inspection, at least five foraminiferal sand layers are recognized (Fig. F11, intervals i–v). Based on the biostratigraphic tie points, the age of this interval is ~1.4 Ma (early Pleistocene) (Keigwin, Rio, Acton, et al., 1998, chap. 5, fig. 66).

Description of X-Radiographic Print. All five visible foraminiferal sand layers have sharp bases (at 117.5 cm [Fig. F12, interval v], 120.3 cm [Fig. F12, interval iv], 121.0 cm [Fig. F12, interval iii], 121.5 cm [Fig. F12, interval ii], and 122.7 cm [Fig. F12, interval i]), suggesting that the flows

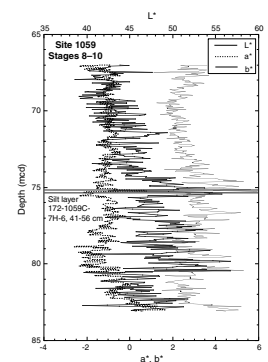
F7. X-radiographic prints showing major erosional surfaces, p. 20.



F8. Magnetic susceptibility variation with depth at Site 1059 during marine isotope Stages 8–10, p. 21.



F9. Color reflectance variation with depth at Site 1056 during marine isotope Stages 8–10, p. 22.



had some degree of intensity. There are many hairline structures between these layers, especially between the upper two layers (117.5–120.3 cm). The lower parts of these foraminiferal sand layers, especially the lower three layers, are relatively unclear because of bioturbation. This means that these five foraminiferal sand layers were not deposited all at once but at intervals between layers. The lowermost part (Fig. F12, interval a) of this sample is massive, bioturbated clay. This clay is truncated very sharply, and there are some hairline structures in a 2-mm interval between the erosional surface of the top of the clay and below the first foraminiferal sand layer (Fig. F12, interval i). This seems to indicate that a fairly intense flow preceded the first sedimentation of carbonate turbidites. The middle 6 cm (Fig. F12, interval b) of this sample consists of the carbonate turbidites described above. The overlying, uppermost part (Fig. F12, interval c) of this sample has obscure line structures that are destroyed by intense bioturbation. The middle foraminiferal sand layers seem to have been deposited quickly compared to the upper and lower parts of this sample.

Site 1064

The sediments of Site 1064 are characterized by sharp color changes (e.g., Keigwin, Rio, Acton, et al., 1998, chap. 6, fig. 7) compared to other deep sites (i.e., Sites 1062 and 1063). The core that contains these samples consists of brown to reddish brown clay. Some of the sharp color changes are overlain by silt laminae or silty intervals (Fig. F13A). Sample 172-1064A-1H-6, 88–103 cm, is taken from the sharp color contact with overlying silt layers, and Sample 172-1064A-1H-4, 120–130 cm, is taken from the sharp color contact without overlying silt layers in the visual inspection (Fig. F13B).

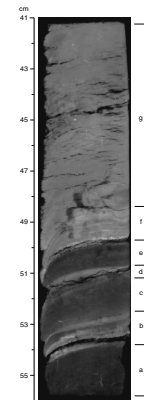
Magnetic susceptibility values show large peaks at both of these sharp contacts (Fig. F14). Color reflectance shows that both a^* and b^* values increase rapidly. On the contrary, L^* values decrease rapidly up-hole (Fig. F15; solid arrows). These changes in color reflectance are common for both samples, although the change in Section 172-1064A-1H-4 is smaller in scale. Moreover, color reflectance indicates other sharp boundaries can be predicted in Section 172-1064A-1H-4 (Fig. F15; dashed arrows). Therefore, this kind of change in color reflectance may indicate the abrupt inflow of sediments associated with the turbidity currents at this site.

Sample 172-1064A-1H-6, 88–103 cm (8.38–8.53 mbsf)

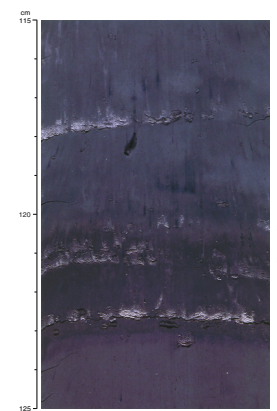
This sample contains a sharp contact between pale brown (2.0Y 4.4/0.8) clay and overlying reddish brown (0.7Y 4.0/0.9) clay. The contact is overlain by visible silt laminae, ~1 mm thick (Fig. F13A).

Description of X-Radiographic Print. The lowermost 2.4-cm interval of this sample is massive (bioturbated?) clay (Fig. F16A, interval a). The upper contact of this clay is sharply truncated. This part is correlatable to the color change (Fig. F13A). A distinct but discontinuous hairline directly overlies the erosional surface. Above this line, visible silt layers appear as two light lines in the radiograph (Fig. F13A, bottom of interval b). The upper line shows a fining-upward structure. Above these lines, at least 12 units of light and dark layers are found in the 8-cm-thick interval (92–100 cm). These structures can be recognized only on the X-radiographic print, not by visual inspection. Distinct fining-upward layers are recognized at 92–93 cm and 97–98 cm. Some of the units have scoured lower boundaries (s marks on Figure F16A at around

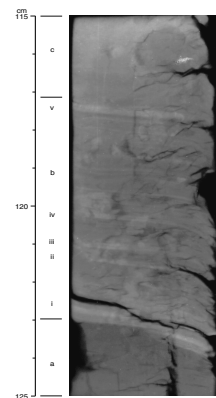
F10. X-radiographic print for Sample 172-1059C-7H-6, 41–56 cm, p. 23.



F11. Close-up photograph containing thin carbonate turbidites, p. 24.



F12. X-radiographic print for Sample 172-1062A-15H-3, 115–125 cm, p. 25.



92.5 and 97.5 cm). These scoured surfaces may indicate bigger pauses in the turbidity currents. The uppermost 2.5-cm interval (Fig. F16A, interval c) of this sample appears to be highly bioturbated.

The interval of this sample seems to be a single event in magnetic susceptibility (Fig. F14), but the X-radiographic print reveals that it consists of several events that occurred in a relatively short time.

Sample 172-1064A-1H-4, 120–130 cm (5.70–5.80 mbsf)

This sample contains a sharp contact (at 125 cm) between reddish brown (0.5Y 4.1/1.1) clay and overlying greenish brown (5.2Y 4.3/0.7) clay. No visible structures are associated with this contact (Fig. F13B).

Description of X-Radiographic Print. The lower 4.9 cm (Fig. F16B, interval a) of this sample is massive (bioturbated?) clay. This clay is truncated sharply by the overlying 2-mm-thick bright line. The base of this line is correlatable to the visible color change. This layer gradually darkens uphole, suggesting a fining-upward structure. In addition to this layer, a 1.9-cm interval above the erosional surface contains at least eight sharp, bright hairlines (Fig. F16B, interval b). The upper contact of this zone is also a sharp boundary, overlain by a 2-mm-thick dark layer (Fig. F16B, interval c), which has a sharp upper contact. Above this contact, the 2.9-cm uppermost part (Fig. F16B, interval d) of this sample is massive (bioturbated?) clay again. The middle 2.1-cm part (Fig. F16B, intervals b, c) of this sample has no bioturbation, suggesting a high sedimentation rate because of the turbidity currents.

This X-radiographic print tells us that sharp color contacts in this site may be accompanied by sharp plane structures derived from turbidity currents, even if these sharp plane structures are not observed by visual inspection.

Group II

Samples in Group II are taken from the sediments deposited during marine isotope Stages 8–10 for the purpose of observing sedimentary structures associated with changes in color or magnetic susceptibility but not associated with visible, distinct structures, as compared to Group I. The samples in this group are considered to represent the more common sedimentary processes in this region.

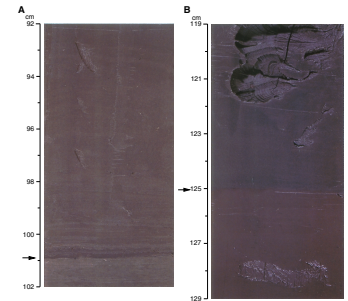
The following X-radiographic print descriptions start at the bases of samples and proceed uphole.

Site 1055

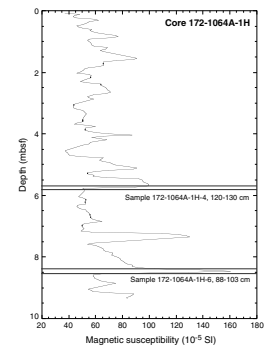
Samples 172-1055D-5H-5, 19–34 cm (46.06–46.21 mcd; Marine Isotope Stage 8); 172-1055C-5H-5, 3–18 cm (48.75– 48.90 mcd; Marine Isotope Stage 8); and 172-1055D-6H-6, 9–24 cm (57.81–57.96 mcd; Marine Isotope Stage 9)

Sample 172-1055D-5H-5, 19–34 cm (Sample 1), is an interval from medium greenish gray (5.4GY 4.5/0.6) clayey silt to medium dark olive-gray (0.8GY 4.2/1.0) silty clay. Sample 172-1055C-5H-5, 3–18 cm (Sample 2), shows no perceptible color change. This sample consists of medium olive-gray silty clay (from 3.2GY 4.1/1.1 to 4.0GY 4.2/1.0 in the uphole direction). Sample 172-1055D-6H-6, 9–24 cm (Sample 3), consists of light greenish gray silty clay. The visible color changes slightly (from 1.5GY 4.9/1.2 to 1.5GY 4.6/1.1 in the uphole direction). The first two samples are located in marine isotope Stage 8, and the third sample is in marine isotope Stage 9. Magnetic susceptibility values increase in

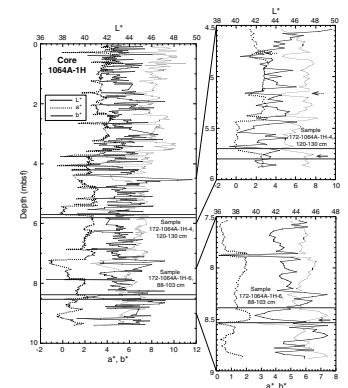
F13. Close-up photographs containing sharp contacts associated with color changes, p. 26.



F14. Magnetic susceptibility variation with depth, p. 27.



F15. Color reflectance variation with depth, p. 28.



the second and third samples and show a small negative peak in the first sample (Fig. F2).

Description of X-Radiographic Print. Sample 172-1055D-6H-6, 9–24 cm, was bioturbated but not as much as were the other two samples (Fig. F17). There are sedimentary structures, but they are obscure in this sample. The lowermost 2.5-cm interval is relatively light in color, which may reflect relatively higher CaCO₃ content, but the upper contact is obscure because of bioturbation. The uppermost 2.5-cm interval of this sample contains obscure dark and light stripes, which suggests that there were primary sedimentary structures, although they have been destroyed by bioturbation.

Sample 172-1055C-5H-5, 3–18 cm, looks homogeneous throughout. No primary sedimentary structures can be observed. Obscure color changes suggesting bioturbation are observed in the lower part of this sample. The upper part is considered to be homogenized by intense bioturbation.

In the lower part of Sample 172-1055D-5H-5, 19–34 cm, a fan-shaped color change is observed. It does not appear to be a primary sedimentary structure but a secondary deformed structure. There is clear trace fossils in this part. The rest of upper part looks homogeneous. There are no distinct primary sedimentary structures, but obscure traces of bioturbation are observed. This may be the result of the intense activity of organisms.

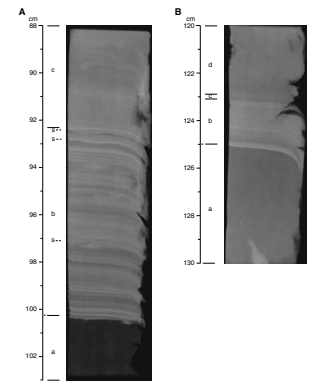
It is notable that the magnetic susceptibility (Fig. F2) and color reflectance (Fig. F3) values are not homogeneous in these 15-cm-long intervals, even though all samples are intensely bioturbated as described above.

Site 1060

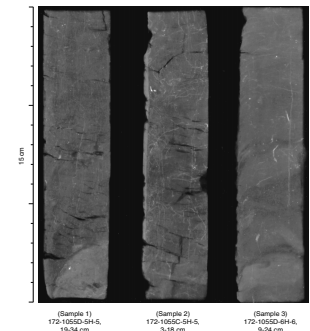
Samples 172-1060C-9H-4, 115–130 cm (86.22–86.37 mcd; Marine Isotope Stage 8); 172-1060A-9H-4, 10–24 cm (92.26–92.41 mcd; Marine Isotope Stage 8); 172-1060B-10H-5, 25–40 cm (100.64–100.79 mcd; Marine Isotope Stage 9); and 172-1060B-10H-6, 9–24 cm (101.98–102.13 mcd; Marine Isotope Stage 10)

Samples 172-1060C-9H-4, 115–130 cm (Sample 1), and 172-1060B-10H-6, 9–24 cm (Sample 4), show no visible color changes, but the change in magnetic susceptibility values is quite large (Fig. F18). In contrast, Samples 172-1060A-9H-4, 10–24 cm (Sample 2), and 172-1060B-10H-5, 25–40 cm (Sample 3), show visible color changes. Sample 4 consists of dark greenish gray clay. No visible color change is observed in this interval (3.8GY 4.5/0.6 to 8.0GY 4.1/0.6). Sample 3 contains color change intervals from reddish brown (2.4GY 4.8/0.6) clay to greenish gray (4.3GY 5.6/0.7) clay with nannofossils. The contact of these lithologies is bioturbated and gradual. Sample 2 also contains a color change interval from relatively light greenish gray (5.7GY 4.9/0.6) nannofossil clay to greenish gray (5.4GY 4.2/0.7) clay with nannofossils. The color change is gradual. Sample 1 is greenish gray clay. There is no visible color change in this interval (5.3GY 4.1/0.3 to 5.1GY 4.0/0.4). L* values change in this interval but not as much as seen in Samples 2 and 3 (Fig. F19). Sample 4 is situated in the end of marine isotope Stage 10. Magnetic susceptibility values reach a slight peak and then decrease abruptly uphole (Fig. F18). Sample 3 is situated in the very beginning of marine isotope Stage 9, where magnetic susceptibility decreases abruptly. Sample 2 is situated ~30 cm above the silt layer, which is in

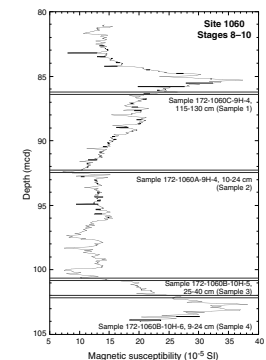
F16. X-radiographic prints showing major erosional and scoured surfaces, p. 29.



F17. X-radiographic prints for samples at Site 1055, p. 30.



F18. Magnetic susceptibility variation with depth at Site 1060 during marine isotope Stages 8–10, p. 31.



marine isotope Stage 8 and can be correlated from Sites 1055 to 1062 (regarding the correlatable silt layer, see previous description of Sample 172-1059C-7H-6, 41–56 cm, in “Site 1059,” p. 6). In Sample 2, we begin to observe the increase in magnetic susceptibility. Sample 1 is situated in marine isotope Stage 8.

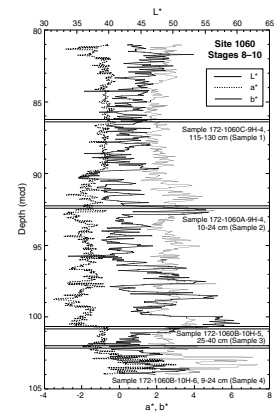
Description of X-Radiographic Print. Sample 4 contains two light lines in the middle (Fig. F20). These lines coincide with the peak in magnetic susceptibility, suggesting the inflow of sediments that have high magnetic susceptibility. However, these lines are not as sharp as the lines seen in Group I, suggesting that the flow is not fast enough to make plane beds or erosional surfaces. Dark and light stripes are also seen in the lowermost 4-cm interval of Sample 4, although it is bioturbated. The lowermost 4 cm of Sample 3, although bioturbated, shows dark and light stripes. The entire sample is highly bioturbated. The uppermost 2.5 cm of the sample shows a slightly lighter color in the radiograph. In Sample 2, the lowermost 5-cm zone of nannofossil clay is relatively light in the X-radiographic print and becomes darker upcore. It is highly bioturbated and homogeneous throughout. White shadows at both ends of the sample may be pyrite pieces. Sample 1 is highly bioturbated and homogeneous throughout. This interval shows a slight peak in magnetic susceptibility but no remaining sedimentary structures. It is notable, here as well as in Site 1055, that the magnetic susceptibility and color reflectance values are not homogeneous in these 15-cm-long intervals, even though the samples are intensely bioturbated as described above.

Site 1062

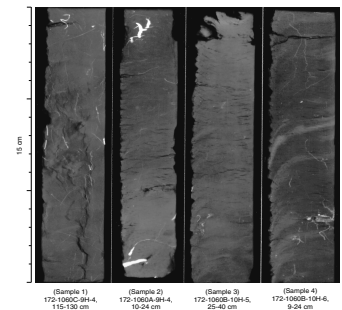
Samples 172-1062B-6H-2, 123–138 cm (45.74–45.89 mbsf: 50.07–50.22 mcd; Marine Isotope Stage 8); 172-1062B-6H-6, 8–23 cm (50.58–50.73 mbsf: 54.92–55.07 mcd; Marine Isotope Stage 9); 172-1062B-6H-6, 46–61 cm (50.96–51.11 mbsf: 55.30–55.45 mcd; Marine Isotope Stage 9); and 172-1062B-7H-3, 117–132 cm (56.67–56.82 mbsf: 56.37–56.52 mcd; Marine Isotope Stage 9)

Samples 172-1062B-6H-2, 123–138 cm (Sample 1), and 172-1062B-7H-3, 117–132 cm (Sample 4), show no visible color changes, but the change in magnetic susceptibility values is quite large, especially in Sample 4 (Fig. F21). In contrast, Samples 172-1062B-6H-6, 8–23 cm (Sample 2), and 172-1062B-6H-6, 46–61 cm (Sample 3), show visible color changes (Fig. F22) related to the nannofossil abundance, which is typically seen in Unit I of Site 1062. Sample 4 consists of olive-gray clay with nannofossils. No visible color change is observed in this interval (3.6Y 3.6/0.4 to 3.3Y 3.4/0.6). Sample 3 contains a color change interval from light olive-gray (8.6Y 5.1/0.8) nannofossil clay to olive-gray (0.9GY 4.7/0.5) clay with nannofossils. The contact of these lithologies is highly bioturbated. Sample 2 also contains a color change interval from olive-gray (1.1GY 4.5/0.6) clay with nannofossils to light olive-gray (3.2GY 5.4/0.8) nannofossil clay mixed sediments. The contact of these lithologies is also highly bioturbated. Sample 1 is olive-gray clay. There is no visible color change in this interval (0.7GY 4.8/0.2 to 2.0GY 4.6/0.4). Sample 4 is situated in the beginning of marine isotope Stage 9. Magnetic susceptibility values reach a large peak at this point and then decrease abruptly uphole. Samples 2 and 3 are also in marine isotope Stage 9. Samples 2 and 3 are on either side of a peak in magnetic susceptibility (Fig. F21). This peak is situated about 3 m below the silt layer that is situated in marine isotope Stage 8 and can be correlated

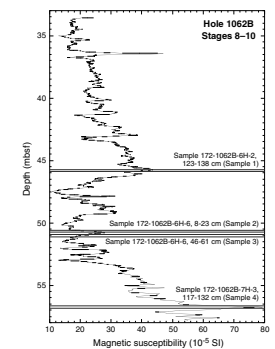
F19. Color reflectance variation with depth at Site 1060 during marine isotope Stages 8–10, p. 32.



F20. X-radiographic prints for samples at Site 1060, p. 33.



F21. Magnetic susceptibility variation with depth in Hole 1062B during marine isotope Stages 8–10, p. 34.



from Sites 1055 to 1062 (regarding the correlatable silt layer, see previous description of Sample 172-1059C-7H-6, 41–56 cm, in “Site 1059,” p. 6). Sample 1 is situated in marine isotope Stage 8.

Description of X-Radiographic Print. Sample 4 is highly bioturbated throughout (Fig. F23). There is only one dark line structure, at 4 cm below the top of the sample. This dark line almost coincides with the large peak in magnetic susceptibility values in this sample. The abrupt increase in magnetic susceptibility could have resulted in more structures, but all other structures presumably have been destroyed by bioturbation. In other words, this kind of peak in magnetic susceptibility is not eliminated by bioturbation. The lower 3.5 cm of Sample 3 is lighter than the upper part in the X-radiographic print. The contact with the upper, darker part is highly bioturbated. At 1.3 cm below the top of the sample is a dark line structure, the only one in the upper dark part of Sample 3. The rest is bioturbated. In Sample 2, the lower 6 cm is darker and the remaining, upper part is light. The lower, darker part is intensely bioturbated, and the contact with the upper part is gradual. At 4–5 cm below the top of the sample, there are many sharp, light-colored hairline structures, suggesting fairly intense flows and high sedimentation rates. The overlying part above these hairline structures also shows traces of line structures, although these are destroyed by bioturbation. The lower half of Sample 1 is bioturbated and homogeneous. There is a pair of sharp, dark lines 8.3 cm from the bottom of the sample. Moreover, dark lines are observed upward every 1 cm, although these lines are not as sharp as the lowermost lines and are sometimes bioturbated. These lines are presumed to coincide with the inflow of the same sediments having high magnetic susceptibility as in Sample 4. Samples 1 and 4 indicate that large peaks of magnetic susceptibility may accompany a change in flow conditions, which in turn can leave sedimentary structures in these fine-grained sediments even if the visible sedimentary structures do not exist. Further investigation is needed to determine the intensity of the flows that make these kinds of structures. Comparing Samples 2 and 3 shows a different pattern related to color change. In Sample 3, the color change is very gradual and bioturbated and is not accompanied by any sharp lines. In contrast, in Sample 2 the color change is associated with sharp hairlines. This difference seems to coincide with the variation in both magnetic susceptibility and color reflectance. The rates of change for both variables are greater in Sample 2. The L^* values decrease in steps in Sample 3 but increase abruptly in Sample 2. This pattern seems common in marine isotope Stage 9 of Site 1062 and may mean that the amount of nannofossils decreases in steps but increases abruptly. In other words, relatively intense inflows of sediments with large amount of nannofossils might result in the hairline structures observed in Sample 2.

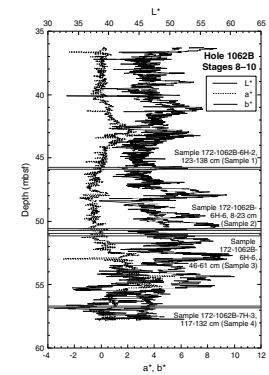
SUMMARY

X-radiographic prints of the slab samples from Leg 172 show the following features.

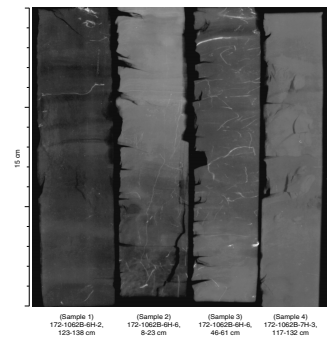
In general, (1) the images become lighter as the amount of nannofossils increases and (2) coarser sediments result in lighter images.

For samples containing visible, distinct structures (Group I), the radiograph images reveal more detailed, fine structures such as (1) distinct sharp lines indicating plane beds; (2) gradation from light to dark uphole, indicating fining-upward structures; (3) ripple cross-laminae;

F22. Color reflectance variation with depth in Hole 1062B during marine isotope Stages 8–10, p. 35.



F23. X-radiographic prints for samples at Site 1062, p. 36.



(4) erosional surfaces sometimes associated with small scours; and (5) very rare bioturbation. These structures indicate fairly intense flows, such as turbidity currents and contour currents, that are especially strengthened by some phenomena (i.e., benthic storms) that occur at these sites and deposit sediments over short periods. Group II samples, which contain visible color changes or changes in magnetic susceptibility but not visibly distinct structures as in Group I, are characterized by (1) bioturbated, gradual contacts; (2) homogeneous images; (3) sharp hairline structures associated with the contacts between the different colors; and (4) obscure line structures that are sometimes bioturbated. It is notable that the sharp peaks in magnetic susceptibility do not disappear even where the interval is intensely bioturbated. It should be noted that the change in color or magnetic susceptibility could be accompanied by some degree of intense flow that could make these line structures in Group II, even though they are not recognized in visual inspections. Although further investigation is needed to discover the intensity of these flows, it is suggested that these changes in flow conditions occur commonly in Deep Western Boundary Currents in these areas, resulting in these kind of structures and the high sedimentation rates seen in our samples. The features observed here would aid our understanding of sedimentation in these areas when linked with studies of other factors, such as isotopes and grain sizes.

ACKNOWLEDGMENTS

X-radiographic prints were made at the Geological Survey of Japan. The author is indebted to Dr. Hajime Katayama and Dr. Yoshiki Saito at the Geological Survey of Japan for their kind instructions and assistance. The author also thanks Dr. Lena Rubensdotter in the Department of Physical Geography, Stockholm University, for her helpful review and Dr. Gary Acton and Lona Dearmont of ODP for their help improving the English and format of the initial version of this manuscript. This research is supported by a grant from the Nissan Science Foundation in 1997.

REFERENCES

- Blum, P., 1997. Physical properties handbook: a guide to the shipboard measurement of physical properties of deep-sea cores. *ODP Tech. Note*, 26 [Online]. Available from World Wide Web: <<http://www-odp.tamu.edu/publications/tnotes/tn26/INDEX.HTM>>. [Cited 1999-07-07]
- Bouma, A.H., 1969. *Methods for the Study of Sedimentary Structures*: New York (Wiley-Interscience).
- Haskell, B.J., Johnson, T.C., and Showers, W.J., 1991. Fluctuations in deep western North Atlantic circulation on the Blake Outer Ridge during the last deglaciation. *Paleoceanography*, 6:21–32.
- Johnson, T.C., Lynch, E.L., Showers, W.J., and Palczuk, N.C., 1988. Pleistocene fluctuations in the western boundary undercurrent on the Blake Outer Ridge. *Paleoceanography*, 3:191–207.
- Keigwin, L.D., and Jones, G.A., 1989. Glacial-Holocene stratigraphy, chronology, and paleoceanographic observations on some North Atlantic sediment drifts. *Deep-Sea Res.*, 36:845–867.
- Keigwin, L.D., Rio, D., Acton, G.D., et al., 1998. *Proc. ODP, Init. Repts.*, 172: College Station, TX (Ocean Drilling Program).
- Munsell Color Company, Inc., 1975. *Munsell Soil Color Charts*: Baltimore, MD (Munsell).
- Nowell, A.R.M., and Hollister, C.D. (Eds.), 1985. Deep ocean sediment transport—preliminary results of the High Energy Benthic Boundary Layer Experiments. *Mar. Geol., Spec. Iss.*, 66.
- Young, M.E.J., 1967. *Radiological Physics*: Illinois (Charles C. Thomas Publ.), 291–332.

Figure F1. Close-up photograph of interval 172-1055D-6H-1, 78–108 cm, containing interbedded silt layers and dark greenish gray clayey silt. The rectangular groove is the trace of the slab sample (172-1055D-6H-1, 84–99 cm).

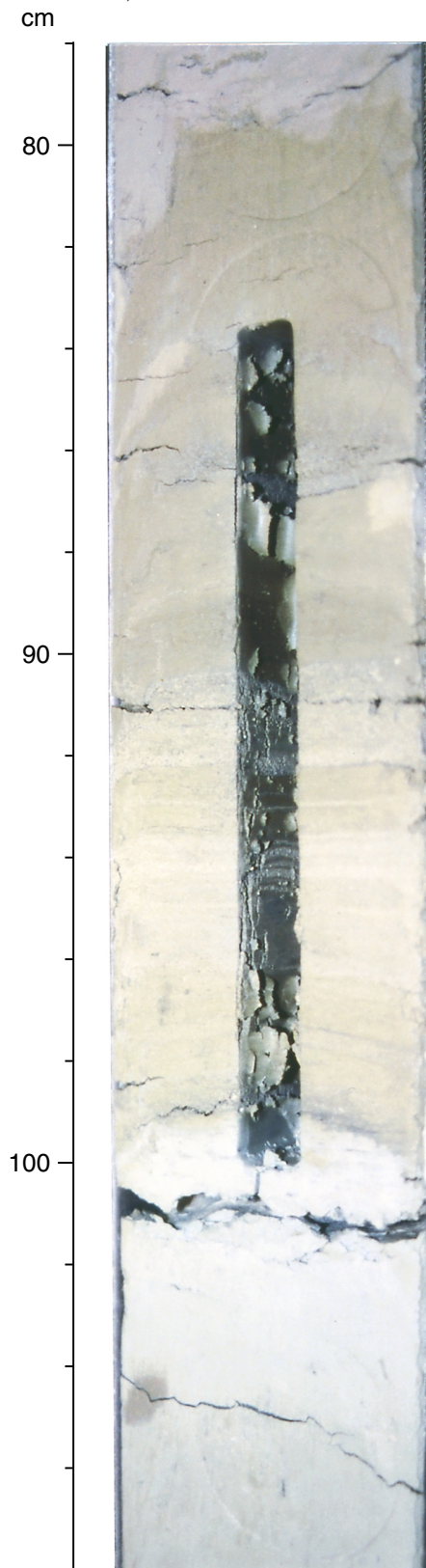


Figure F2. Magnetic susceptibility variation with depth at Site 1055 during marine isotope Stages 8–10. The intervals between horizontal lines indicate the locations of the slab samples.

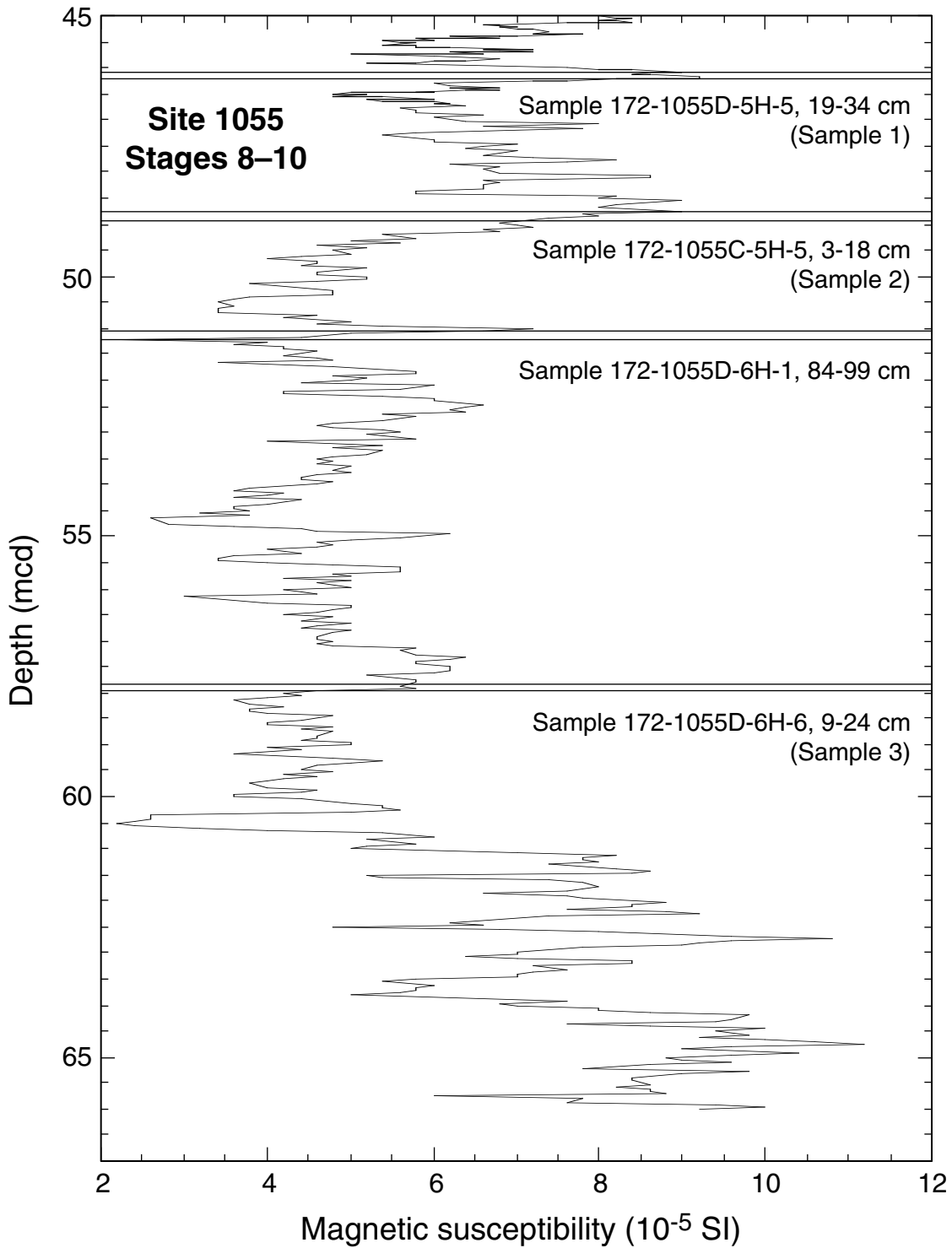


Figure F3. Color reflectance variation with depth at Site 1055 during marine isotope Stages 8–10. The intervals between horizontal lines indicate the locations of the slab samples.

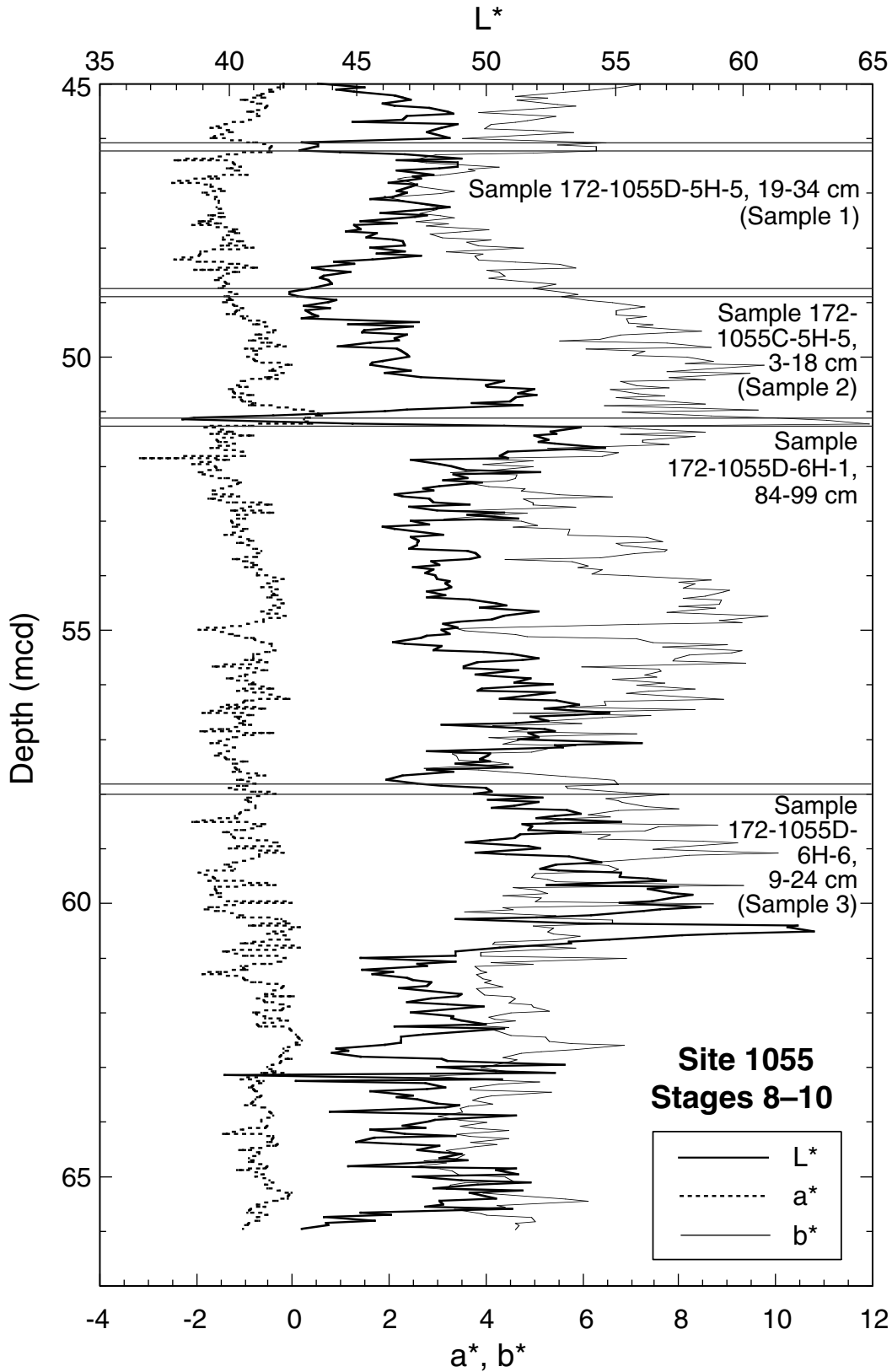


Figure F4. X-radiographic print for Sample 172-1055D-6H-1, 84–99 cm. Asterisks show major erosional surfaces (see “Description of X-Radiographic Print,” p. 4, in “Site 1055” in “Group I” for a detailed description).

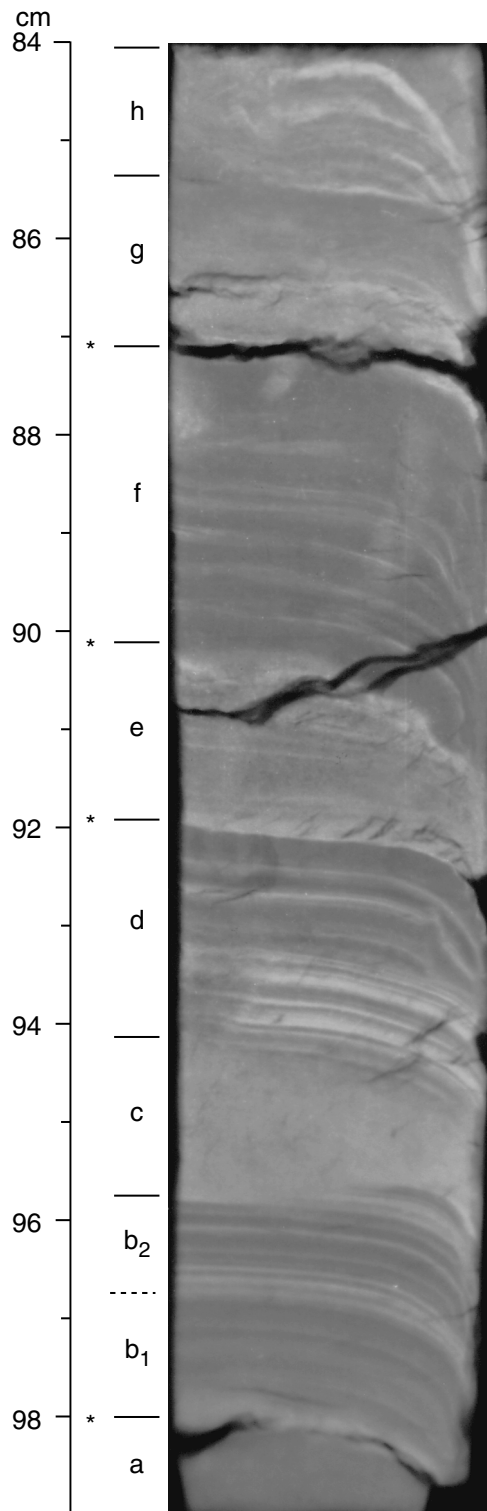


Figure F5. Close-up photograph of interval 172-1056B-6H-5, 47–83 cm, containing a sequence of coarser beds of sand-sized siliciclastic and biogenic components interbedded with silt and clay. The rectangular grooves are the traces of the slab samples (Samples 172-1056B-6H5, 51–66 and 69–79 cm).

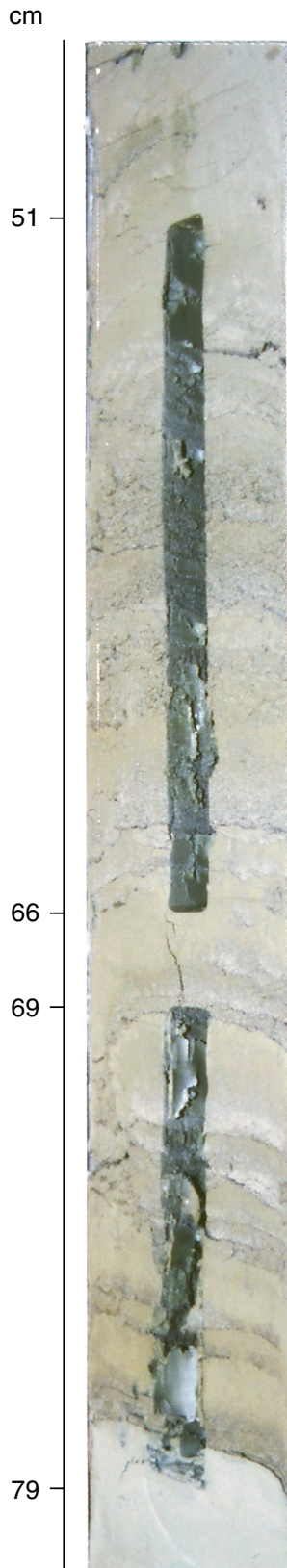


Figure F6. Magnetic susceptibility variation with depth of Core 172-1056B-6H. The interval between horizontal lines indicates the locations of the slab samples.

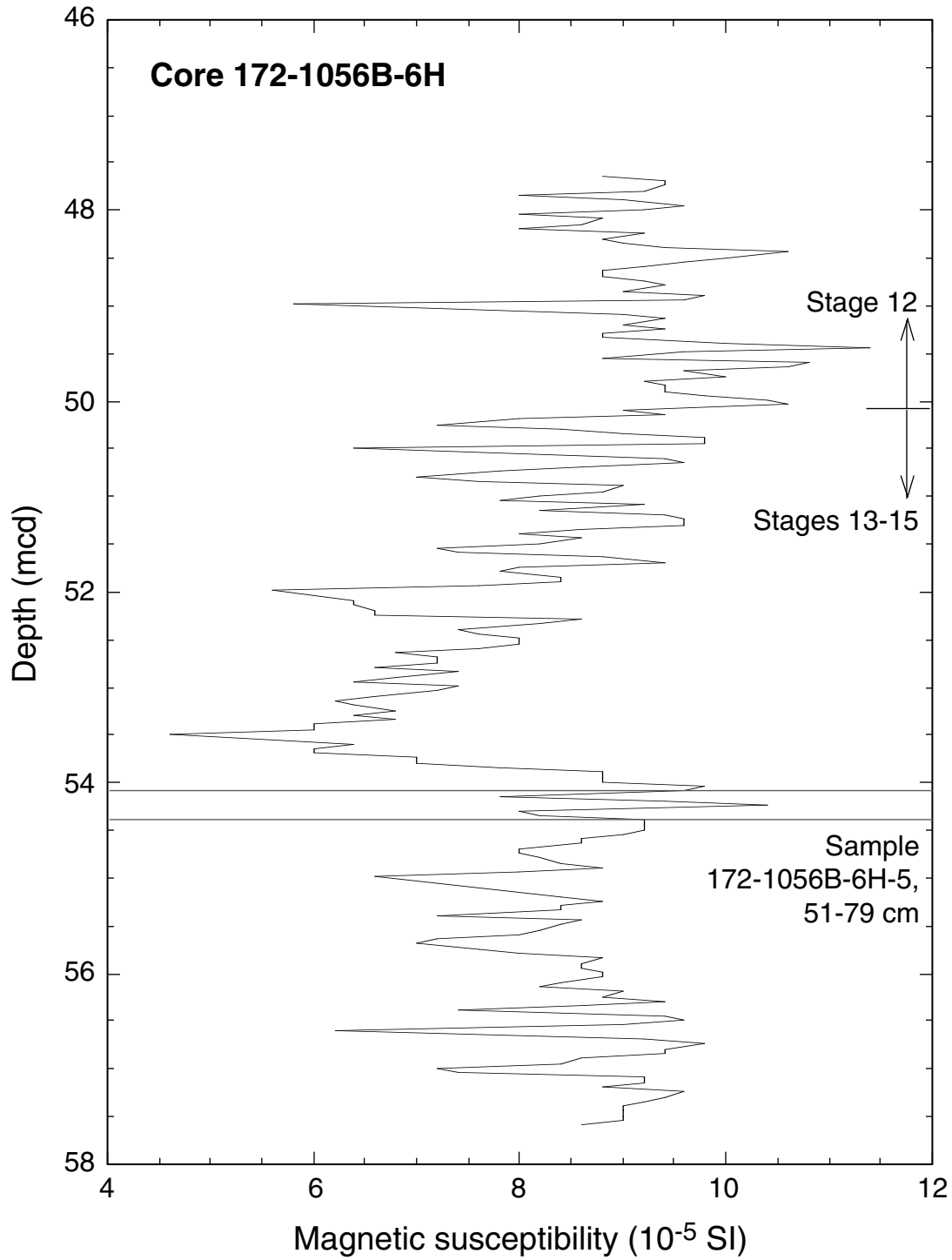


Figure F7. X-radiographic prints for Samples (A) 172-1056B-6H-5, 51–66 cm, and (B) 172-1056B-6H-5, 69–79 cm. Asterisks show major erosional surfaces (see “Description of X-Radiographic Print,” p. 5, in “Site 1056” in “Group I” for a detailed description).

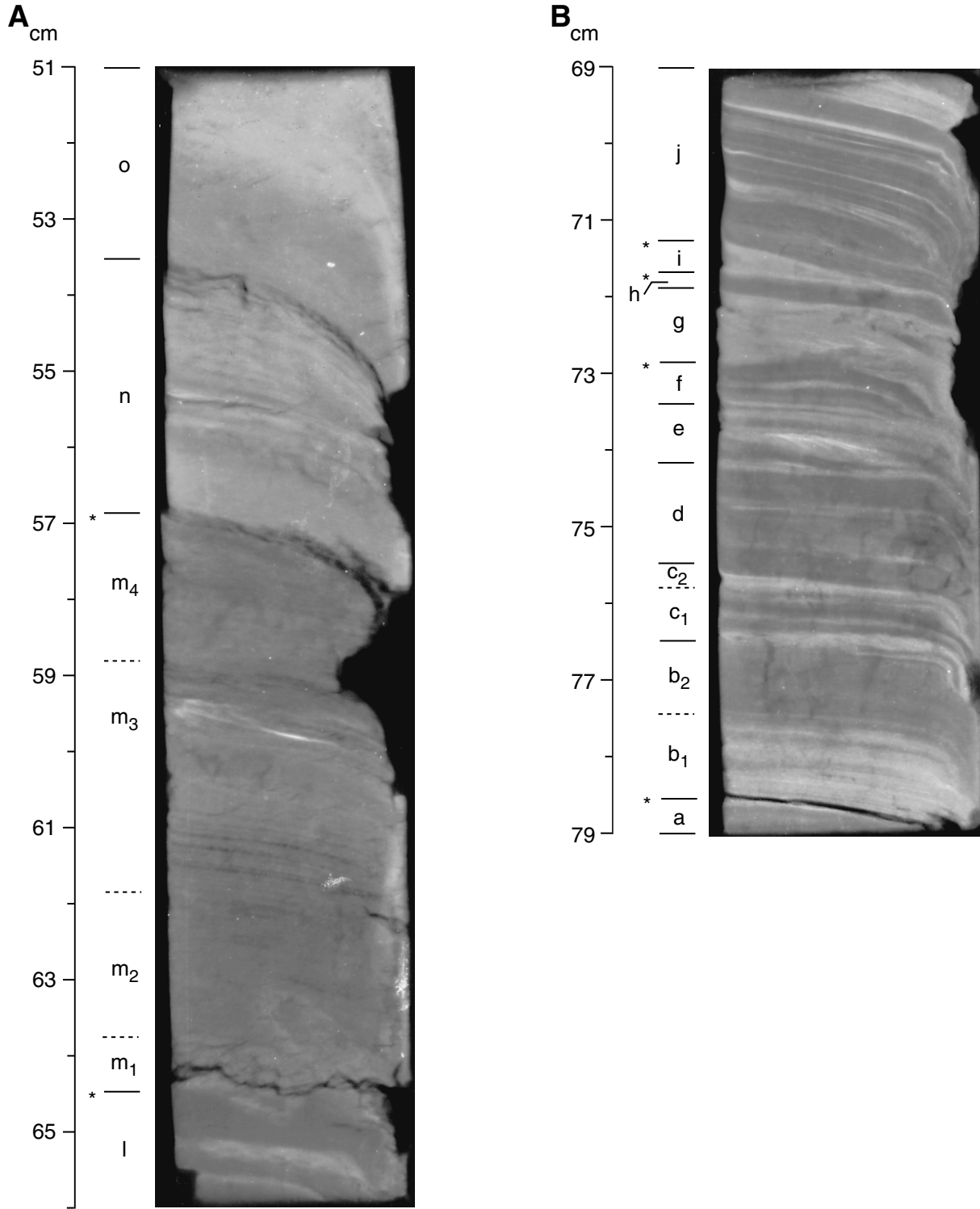


Figure F8. Magnetic susceptibility variation with depth at Site 1059 during marine isotope Stages 8–10. The interval between horizontal lines indicates the location of the slab sample.

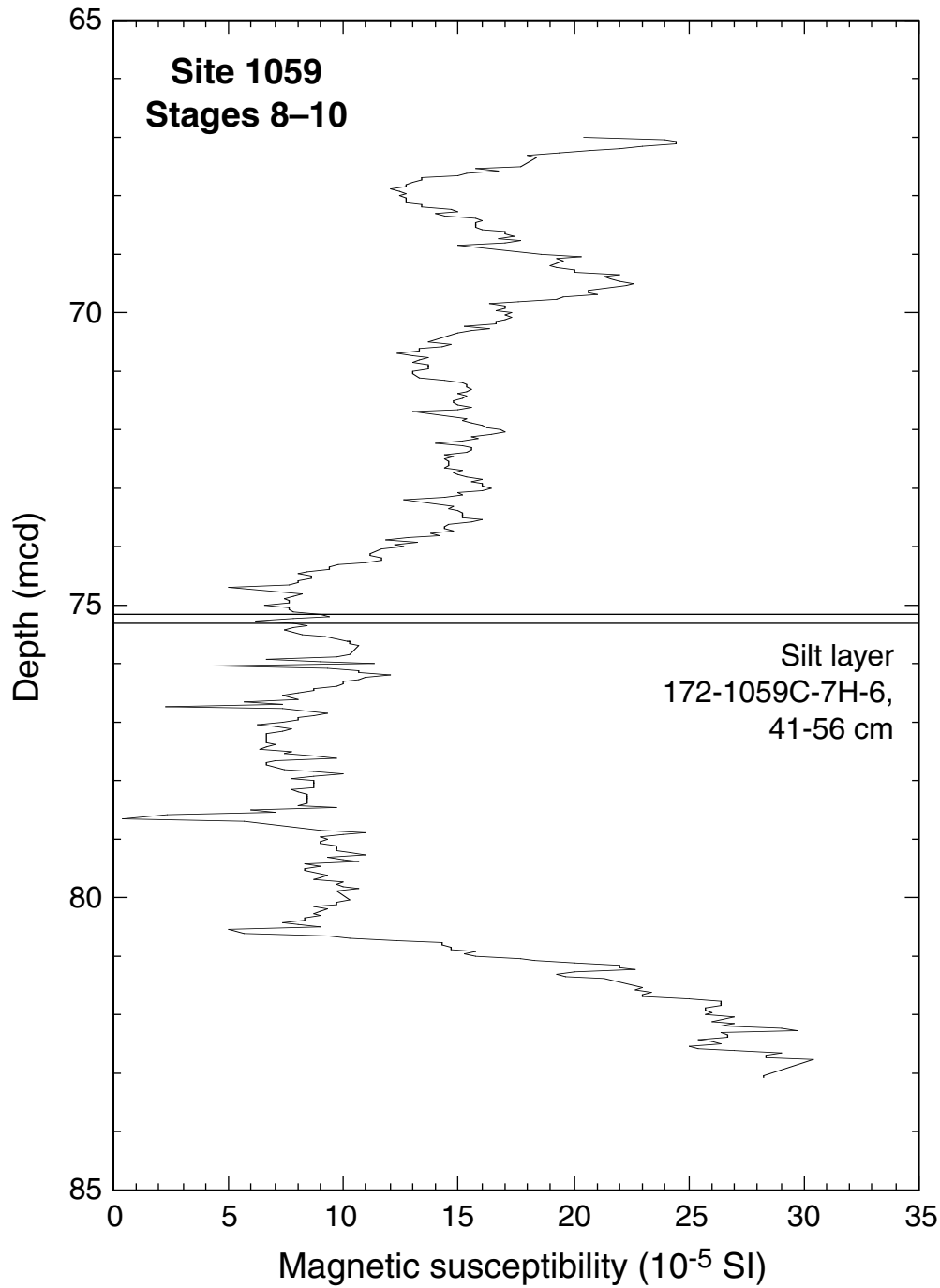


Figure F9. Color reflectance variation with depth at Site 1059 during marine isotope Stages 8–10. The interval between horizontal lines indicates the location of the slab sample.

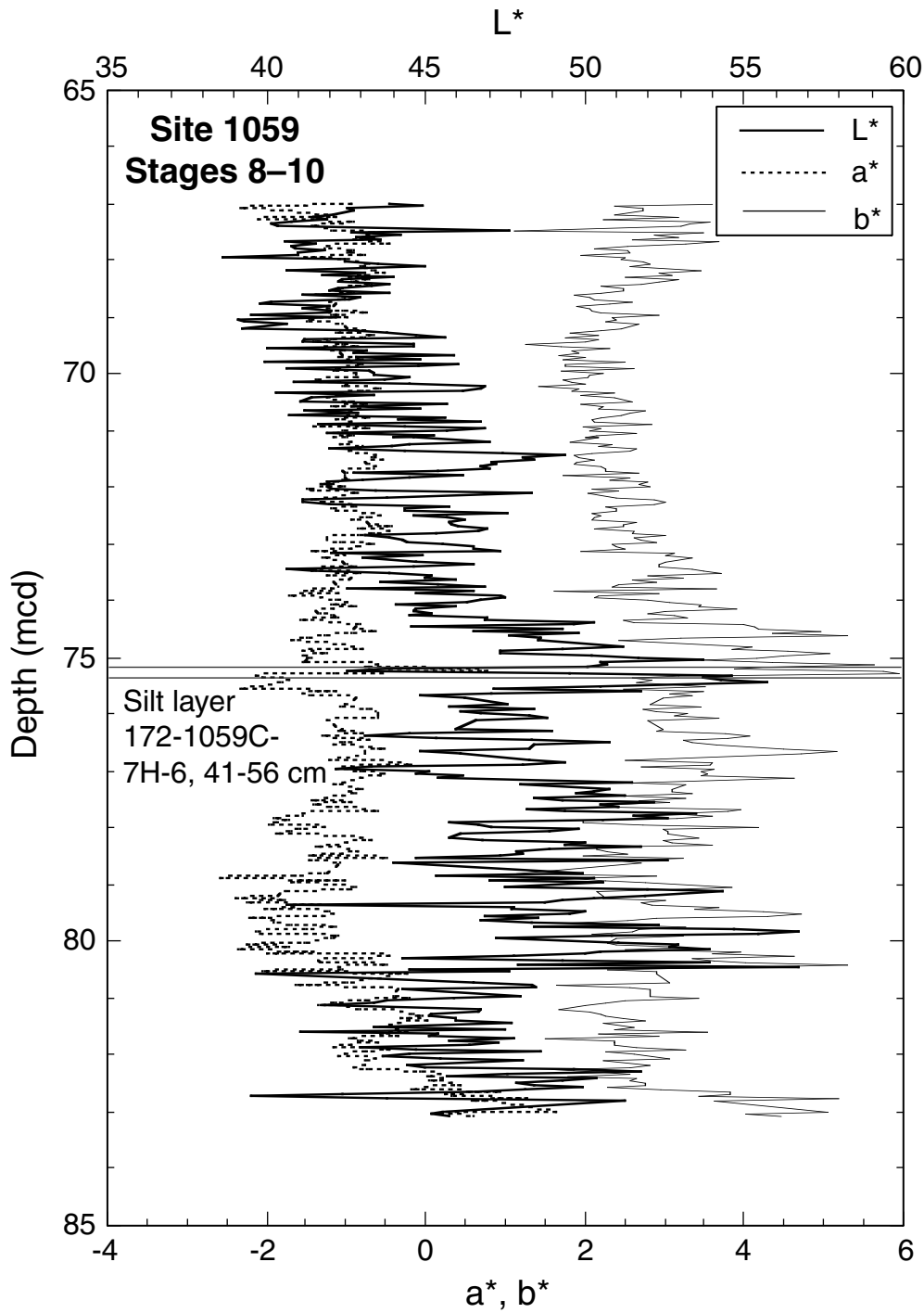


Figure F10. X-radiographic print for Sample 172-1059C-7H-6, 41–56 cm (see “Description of X-Radiographic Print,” p. 6, in “Site 1059” in “Group I” for a detailed description).

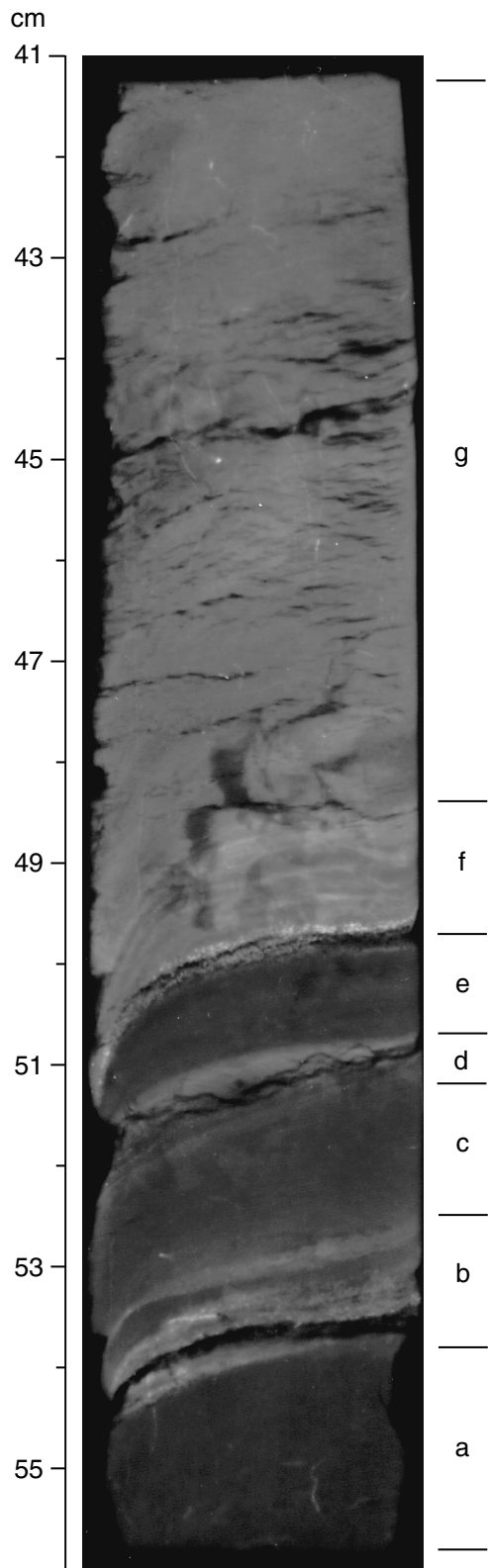


Figure F11. Close-up photograph of interval 172-1062A-15H-3, 115–125 cm, containing thin carbonate turbidites (intervals i–v).

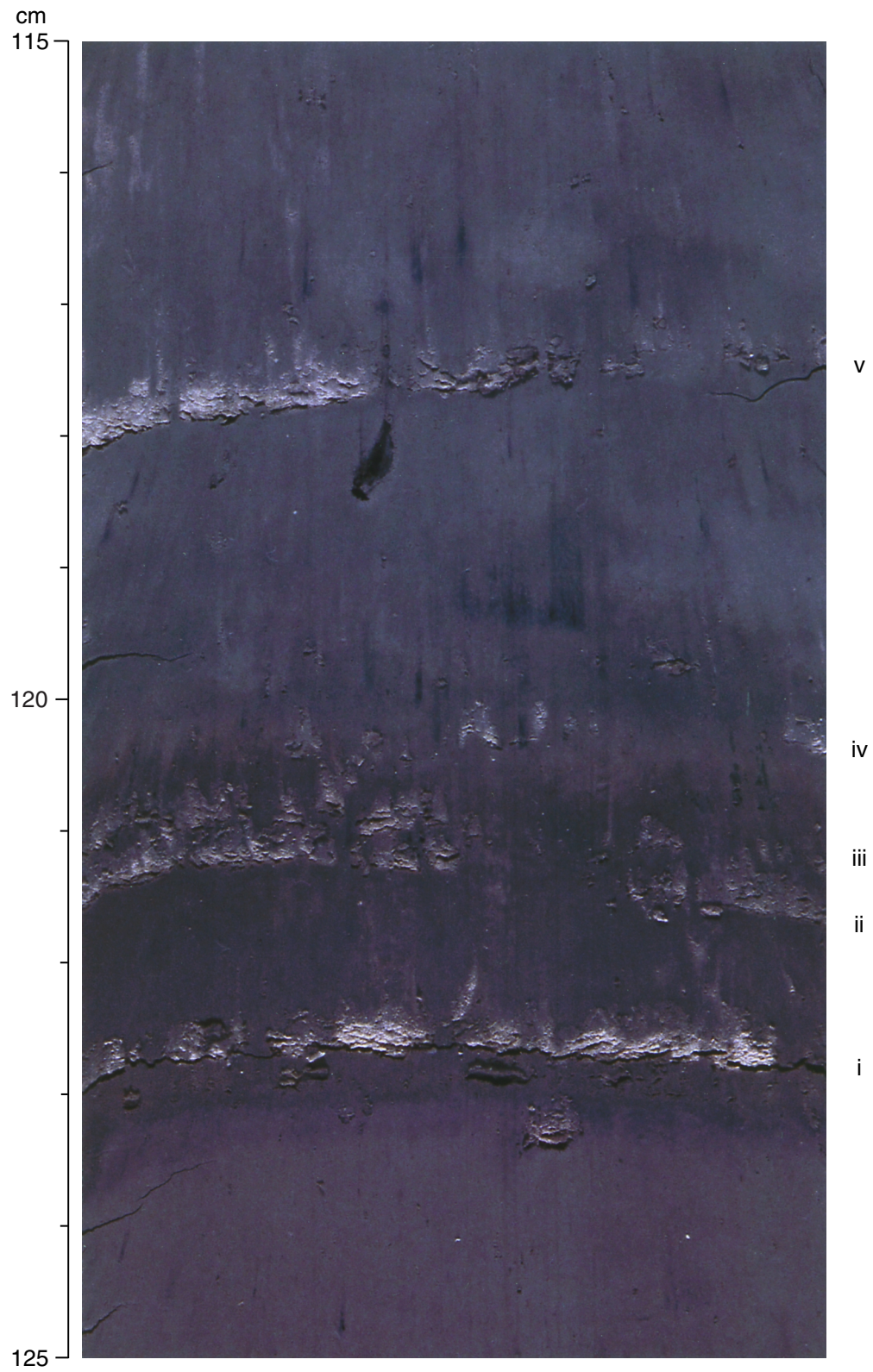


Figure F12. X-radiographic print for Sample 172-1062A-15H-3, 115–125 cm (see “Description of X-Radiographic Print,” p. 6, in “Site 1062” in “Group I” for a detailed description). The letters show the positions of carbonate turbidites and correlate to those in Fig. F11, p. 24.

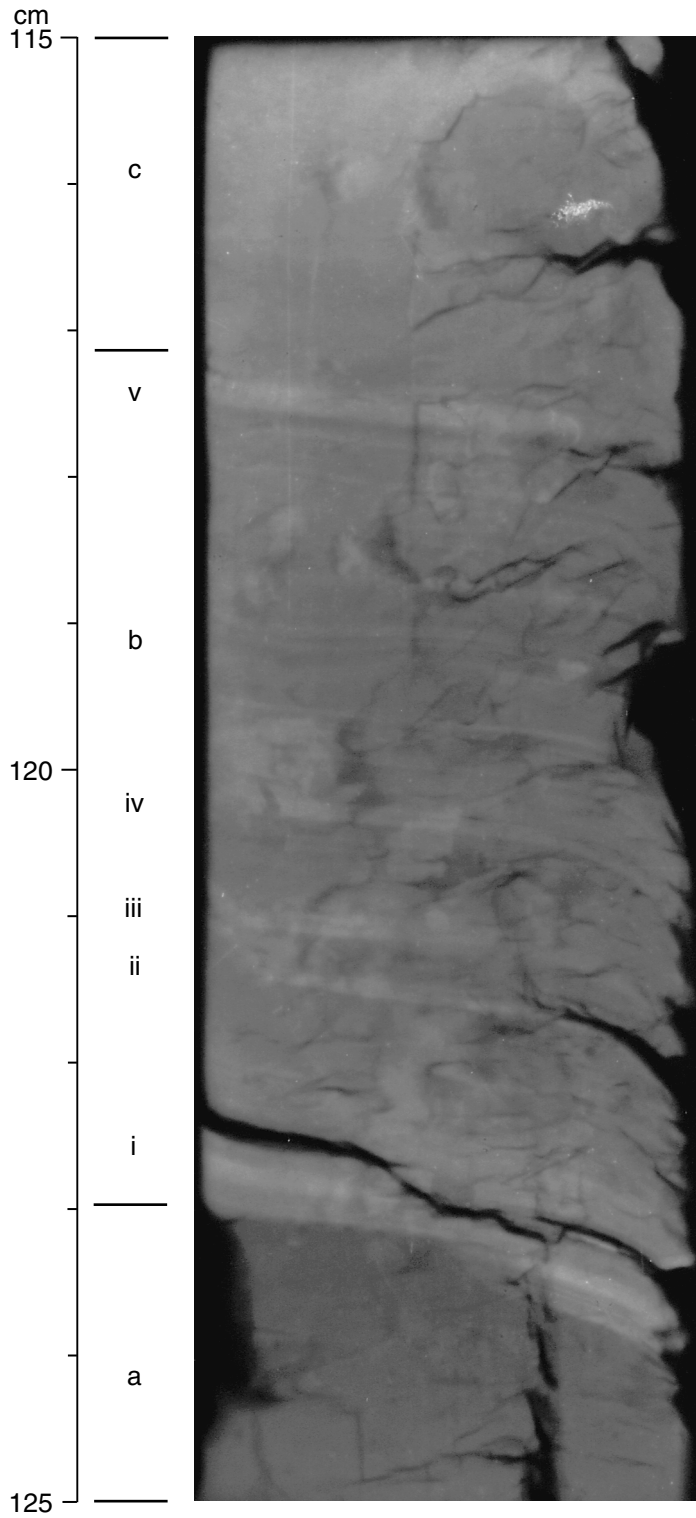


Figure F13. Close-up photographs of intervals (A) 172-1064A-1H-6, 92–102 cm, and (B) 172-1064A-1H-4, 119–129 cm, containing sharp contacts (indicated by arrows) associated with color changes. (A) shows a sharp contact (arrow) overlain by visible silt laminae, each about 1 mm thick. (B) shows a sharp contact (at 125 cm) that is not associated with any visible structure.

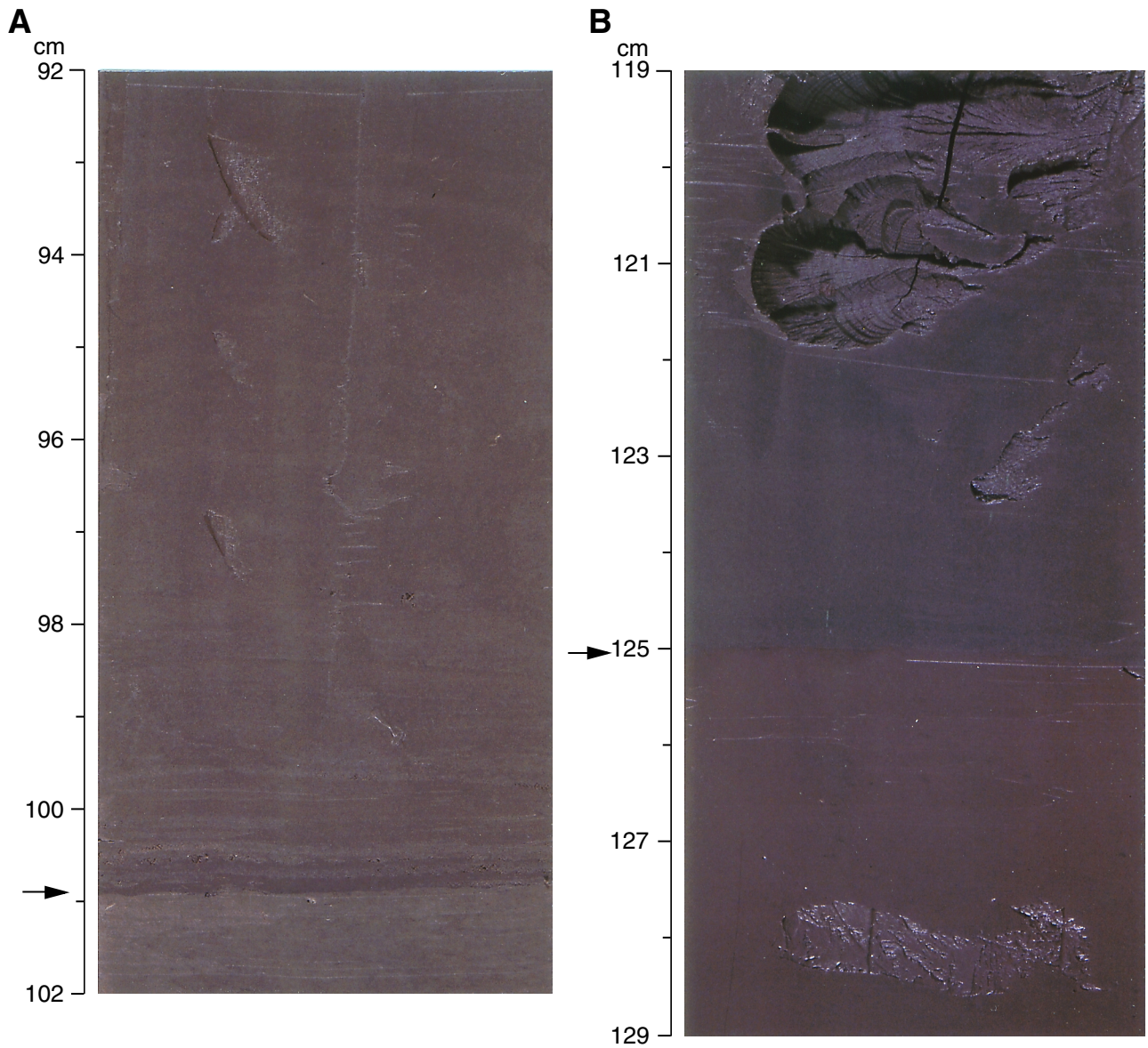


Figure F14. Magnetic susceptibility variation with depth of Core 172-1064A-1H. The intervals between horizontal lines indicate the locations of the slab samples.

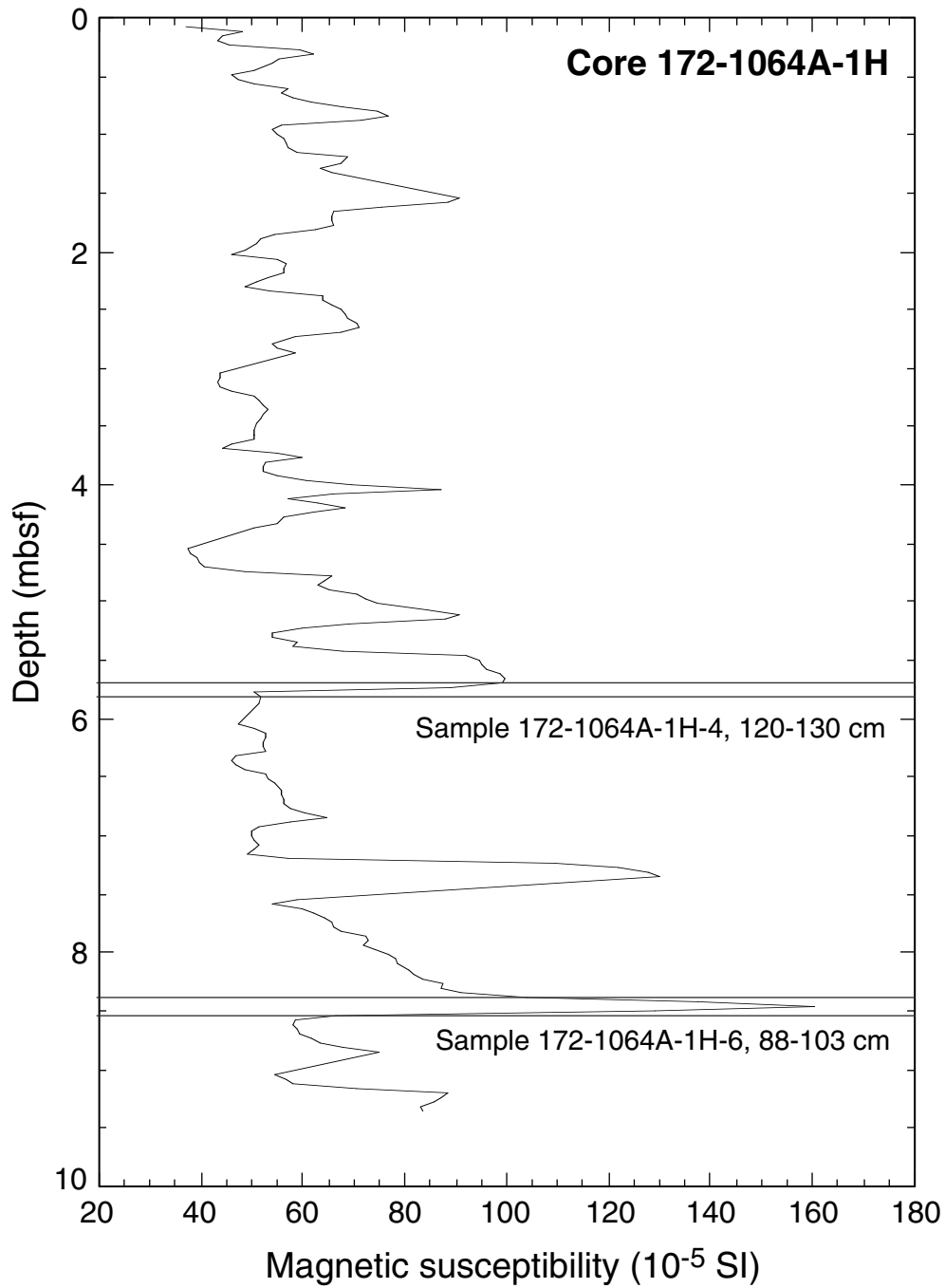


Figure F15. Color reflectance variation with depth of Core 172-1064A-1H. The intervals between horizontal lines indicate the locations of the slab samples.

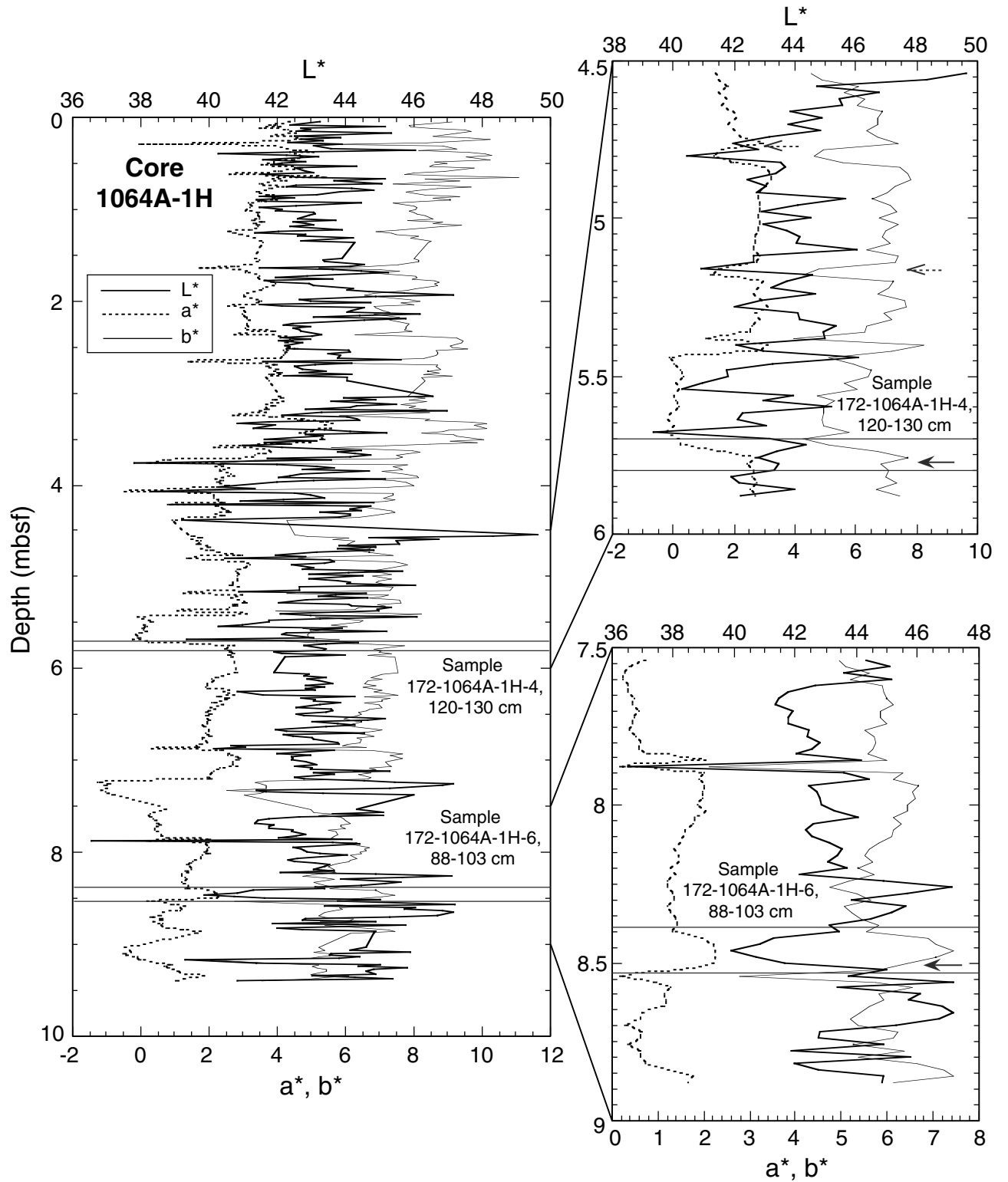


Figure F16. X-radiographic prints for Samples (A) 172-1064A-1H-6, 88–103 cm, and (B) 172-1064A-1H-4, 120–130 cm. Asterisks show major erosional surfaces and s marks show scoured surfaces (see “Description of X-Radiographic Print,” p. 7, in “Site 1064” in “Group I” for a detailed description).

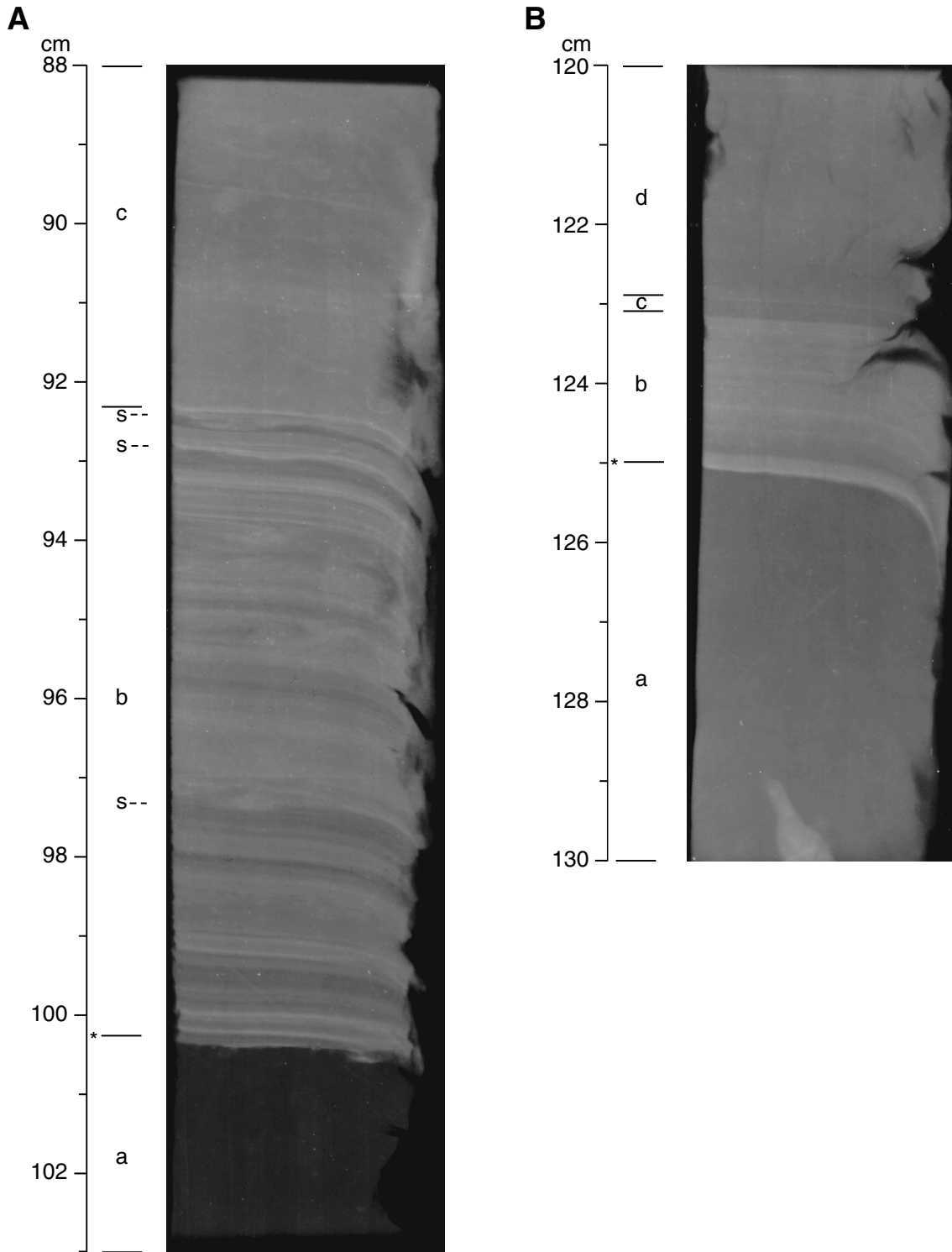


Figure F17. X-radiographic prints for Samples 172-1055D-5H-5, 19–34 cm; 172-1055C-5H-5, 3–18 cm; and 172-1055D-6H-6, 9–24 cm (see “Description of X-Radiographic Print,” p. 9, in “Site 1055” in “Group II” for a detailed description).

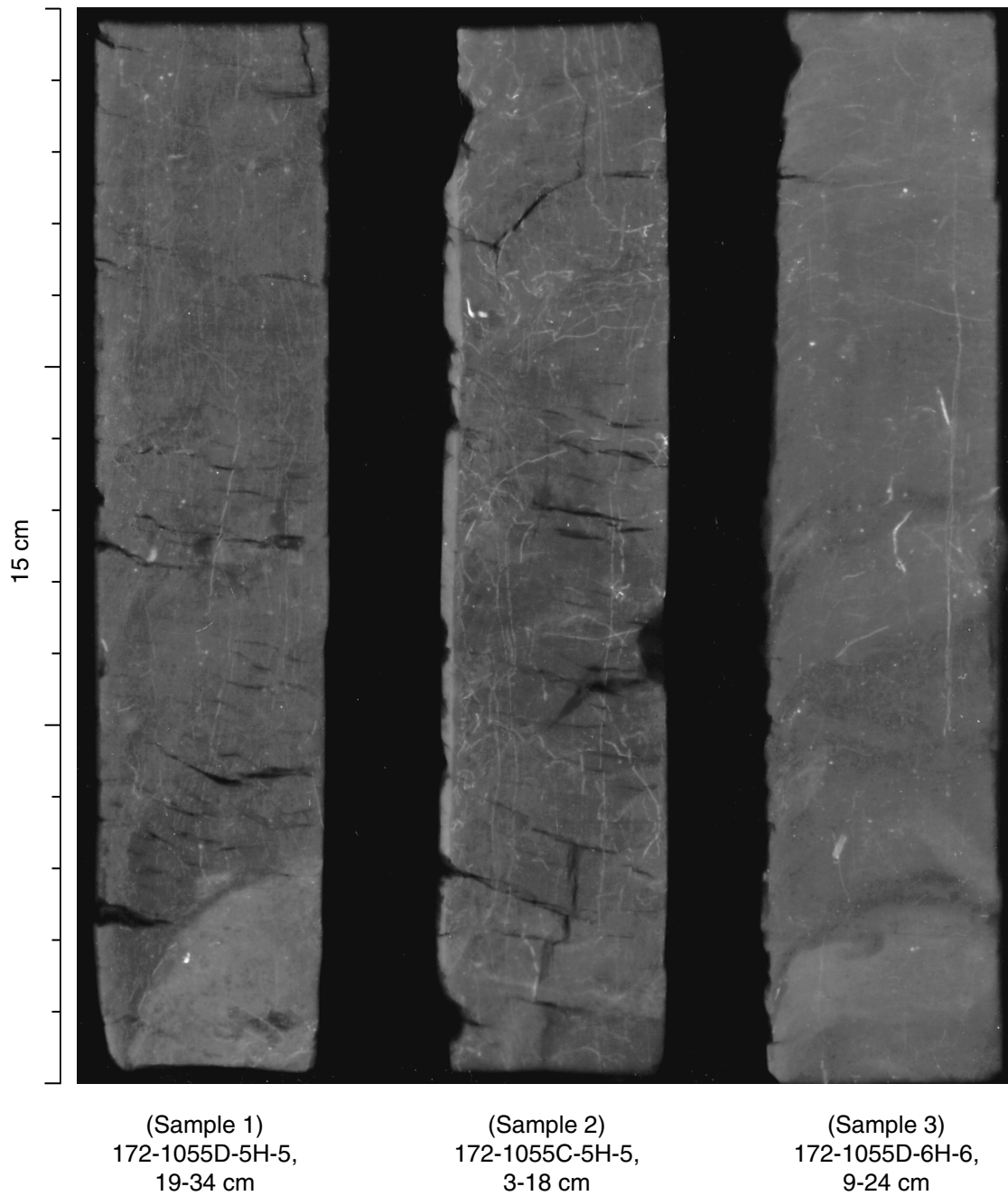


Figure F18. Magnetic susceptibility variation with depth at Site 1060 during marine isotope Stages 8–10. The intervals between horizontal lines indicate the locations of the slab samples.

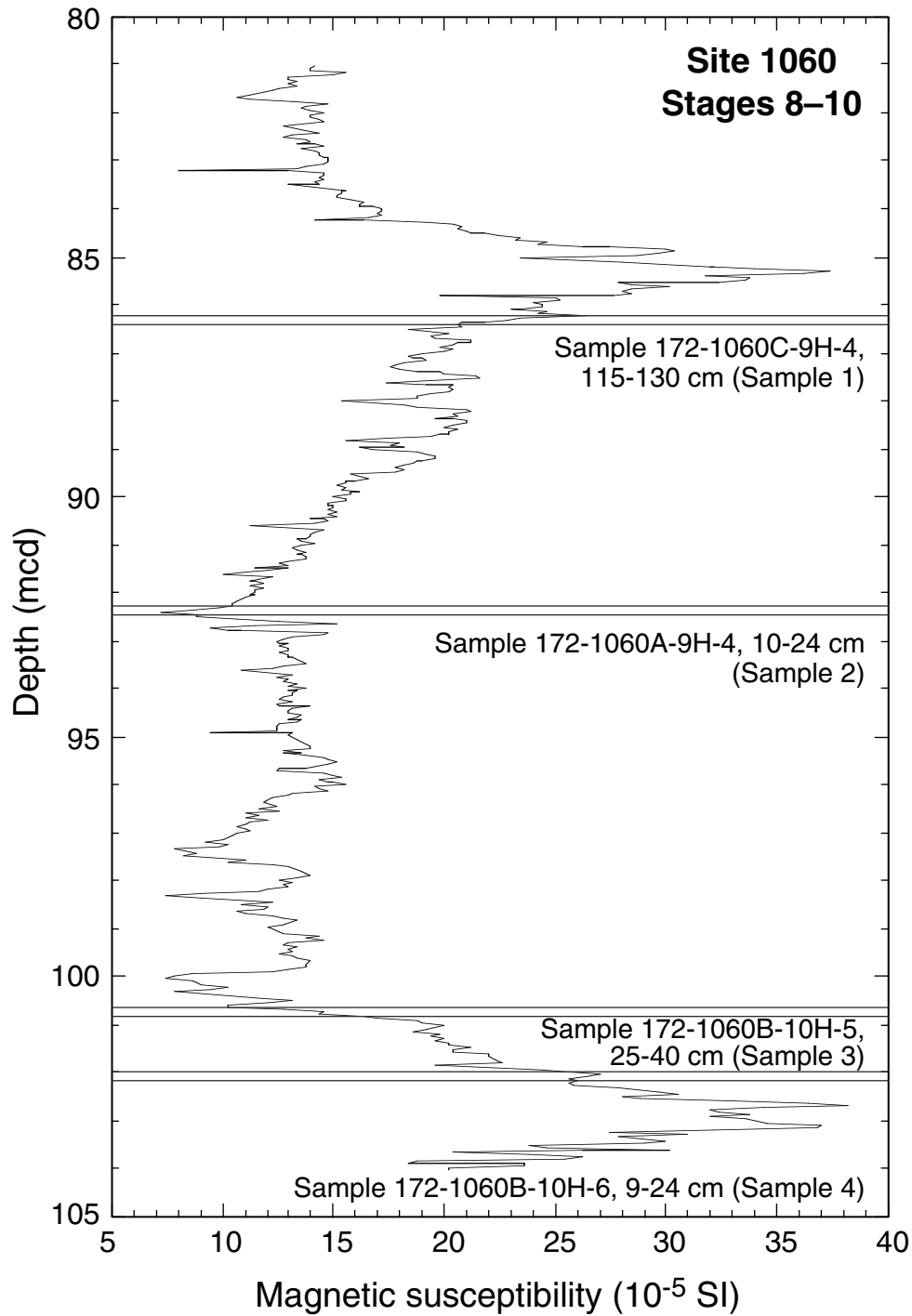


Figure F19. Color reflectance variation with depth at Site 1060 during marine isotope Stages 8–10. The intervals between horizontal lines indicate the locations of the slab samples.

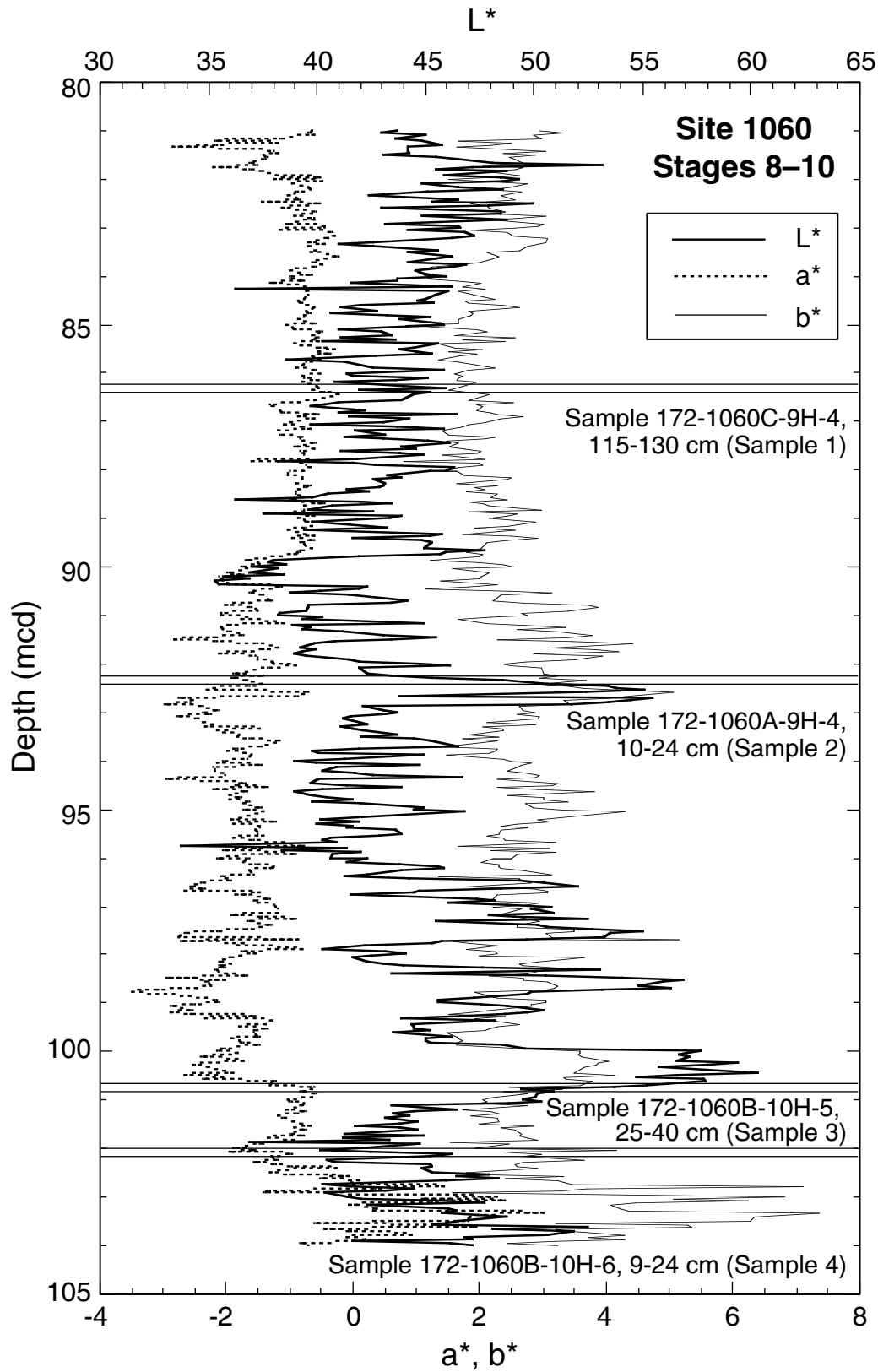


Figure F20. X-radiographic prints for Samples 172-1060C-9H-4, 115–130 cm; 172-1060A-9H-4, 10–24 cm; 172-1060B-10H-5, 25–40 cm; and 172-1060B-10H-6, 9–24 cm (see “Description of X-Radiographic Print,” p. 10, in “Site 1060” in “Group II” for a detailed description).

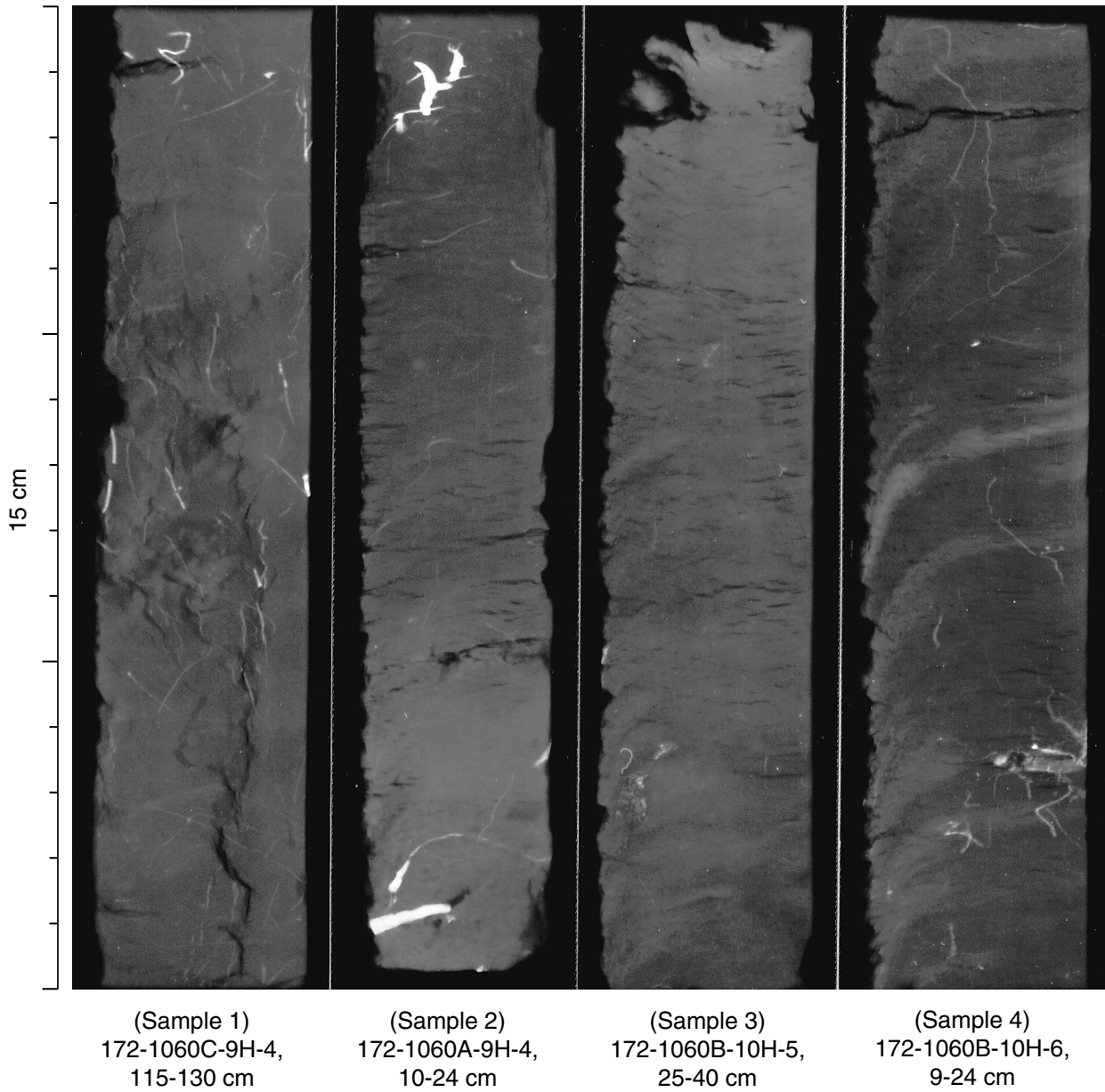


Figure F21. Magnetic susceptibility variation with depth in Hole 1062B during marine isotope Stages 8–10. The intervals between horizontal lines indicate the locations of the slab samples.

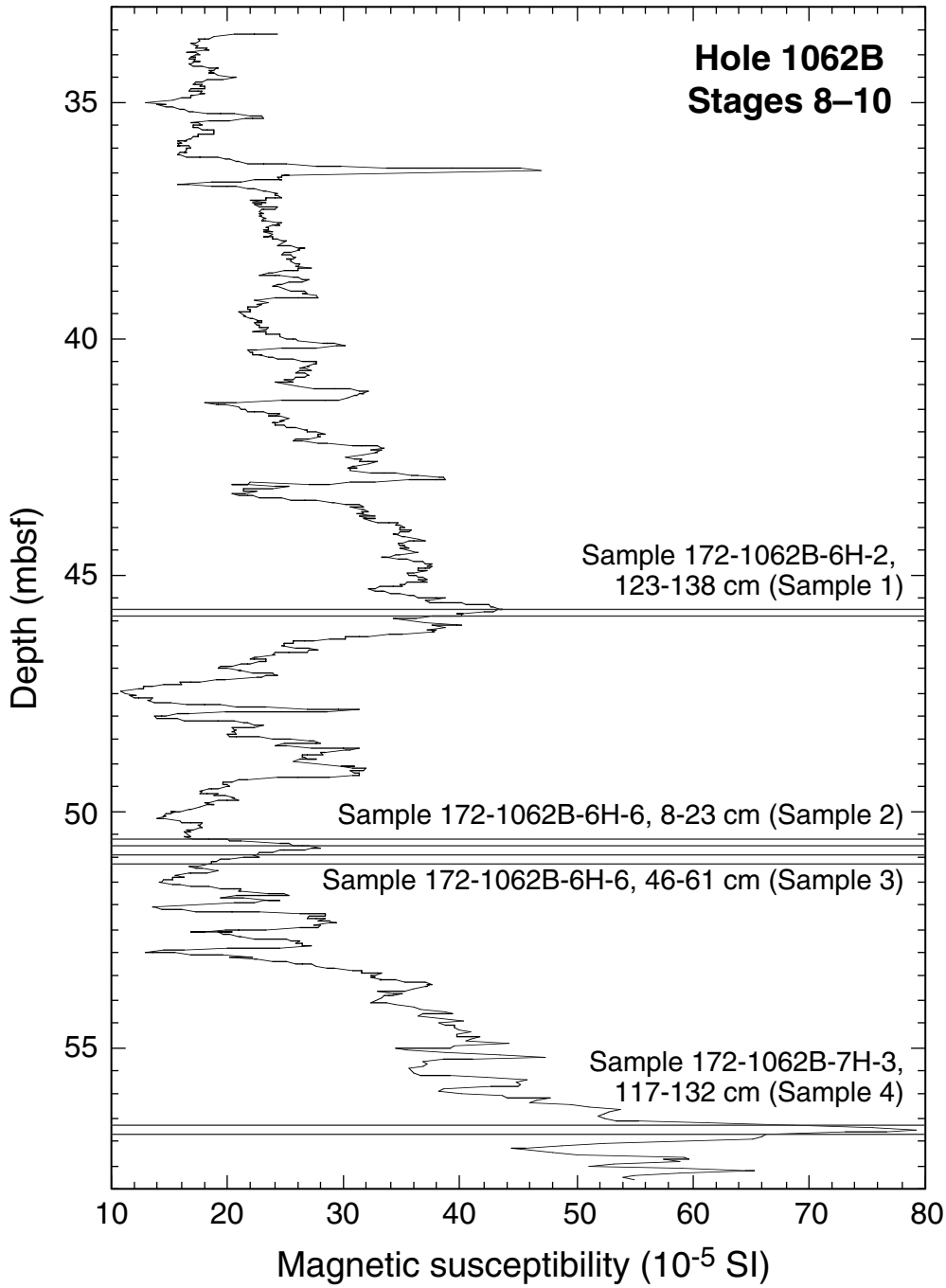


Figure F22. Color reflectance variation with depth in Hole 1062B during marine isotope Stages 8–10. The intervals between horizontal lines indicate the locations of the slab samples.

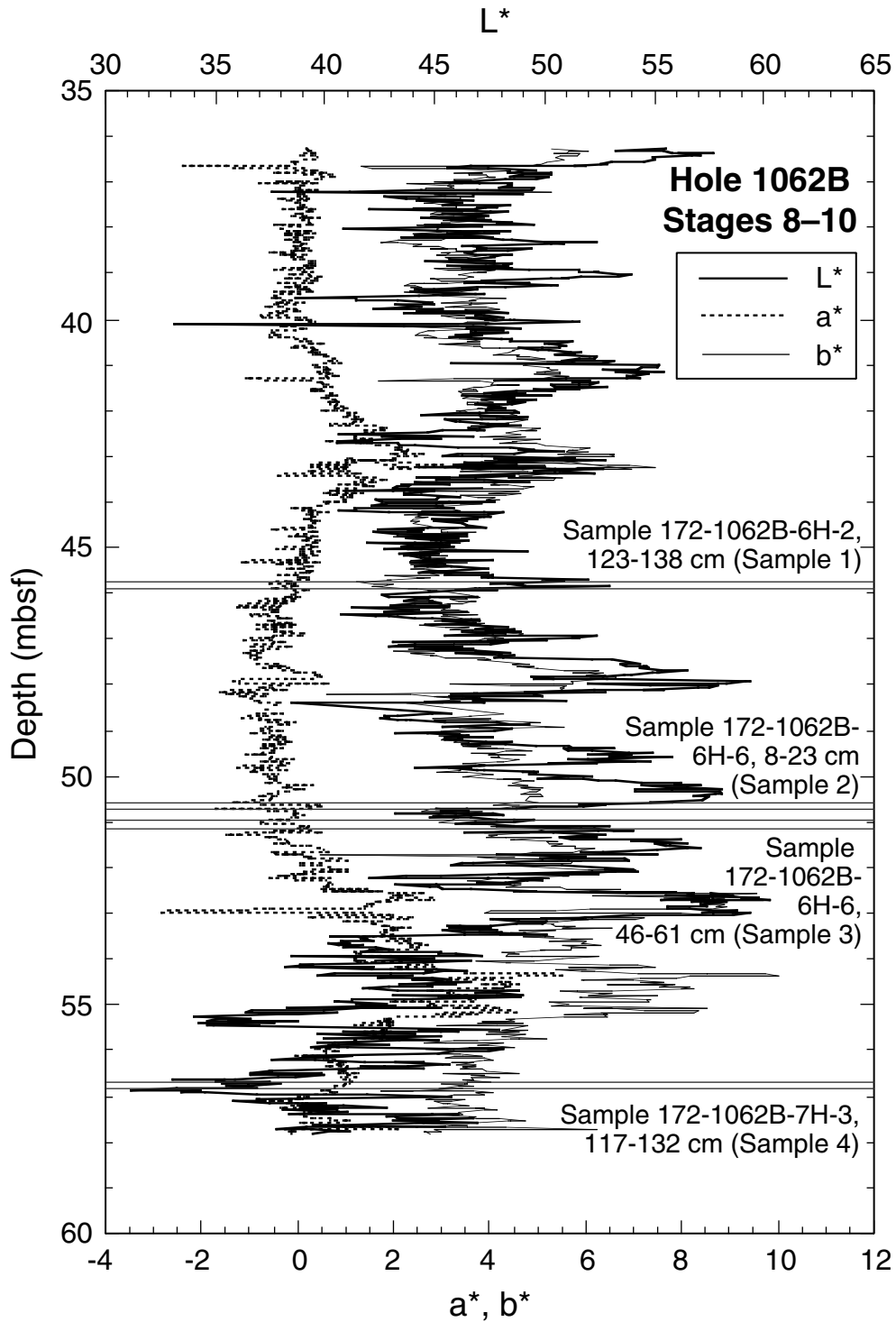
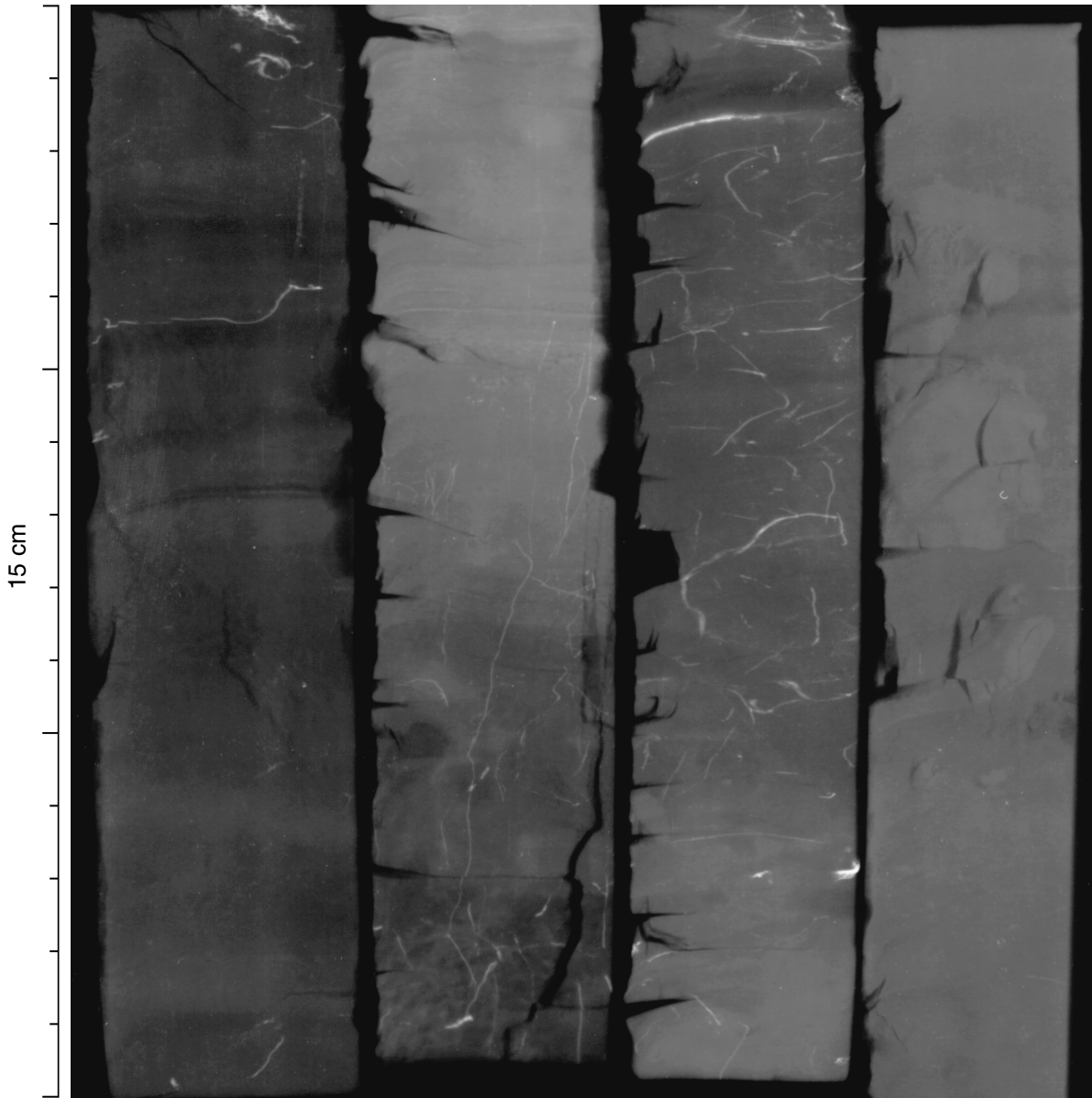


Figure F23. X-radiographic prints for Samples 172-1062B-6H-2, 123–138 cm; 172-1062B-6H-6, 8–23 cm; 172-1062B-6H-6, 46–61 cm; and 172-1062B-7H-3, 117–132 cm (see “Description of X-Radiographic Print,” p. 11, in “Site 1062” in “Group II” for a detailed description).



(Sample 1)
172-1062B-6H-2,
123-138 cm

(Sample 2)
172-1062B-6H-6,
8-23 cm

(Sample 3)
172-1062B-6H-6,
46-61 cm

(Sample 4)
172-1062B-7H-3,
117-132 cm

Table T1. List of slab samples and conditions of X-radiographic prints.

	Leg, hole, core, section, interval (cm)	Exposure conditions for X-radiographs
Group I	172-1055D-6H-1, 84-99	45 kV, 4 mA, 40 s
	172-1056B-6H-5, 51-66	45 kV, 4 mA, 40 s
	172-1056B-6H-5, 69-79	45 kV, 4 mA, 30 s
	172-1059C-7H-6, 41-56	36 kV, 4 mA, 225 s
	172-1062A-15H-3, 115-125	45 kV, 4 mA, 50 s
	172-1064A-1H-4, 120-130	45 kV, 4 mA, 40 s
	172-1064A-1H-6, 88-113	45 kV, 4 mA, 40 s
Group II	172-1055D-5H-5, 19-34	40 kV, 4 mA, 80 s
	172-1055C-5H-5, 3-18	40 kV, 4 mA, 80 s
	172-1055D-6H-6, 9-24	40 kV, 4 mA, 80 s
	172-1060C-9H-4, 115-130	40 kV, 4 mA, 75 s
	172-1060A-9H-4, 10-24	40 kV, 4 mA, 75 s
	172-1060B-10H-5, 25-40	40 kV, 4 mA, 75 s
	172-1060B-10H-6, 9-24	40 kV, 4 mA, 75 s
	172-1062B-6H-2, 123-138	36 kV, 4 mA, 160 s
	172-1062B-6H-6, 8-23	36 kV, 4 mA, 160 s
	172-1062B-6H-6, 46-61	36 kV, 4 mA, 160 s
	172-1062B-7H-3, 117-132	36 kV, 4 mA, 160 s

Notes: Group I samples were collected aboard ship. Group II samples were obtained from the Bremen Core Repository.